Mechanistic analysis of massive endocytosis in relation to functionally defined surface membrane domains

Donald W. Hilgemann and Michael Fine

Department of Physiology, University of Texas Southwestern Medical Center at Dallas, Dallas, TX 75390

A large fraction of endocytosis in eukaryotic cells occurs without adaptors or dynamins. Here, we present evidence for the involvement of lipid domains in massive endocytosis (MEND) activated by both large Ca transients and amphipathic compounds in baby hamster kidney and HEK293 cells. First, we demonstrate functional coupling of the two MEND types. Ca transients can strongly facilitate detergent-activated MEND. Conversely, an amphipath with dual alkyl chains, ditridecylphthalate, is without effect in the absence of Ca transients but induces MEND to occur within seconds during Ca transients. Ca transients, like amphipaths, enhance the extraction of lipids from cells by β-cyclodextrins. Second, we demonstrate that electrical and/or optical signals generated by selected membrane probes are nearly insensitive to MEND, suggesting that those probes segregate into membrane domains that are not taken up by MEND. Triphenylphosphoniums are increasingly excluded from domains that internalize as the carbon chain length increases from 4 to 12. The small cationic membrane dye, FM 4–64, binds well to domains that internalize, whereas a closely related dye with a larger hydrophobic moiety, di-4-ANEPPDHQ (ANEPPDHQ) is excluded. Multiple carrier-type ionophores and a small amphipathic anion, niflumic acid, are also excluded. Probes with modest MEND sensitivity include the hydrophobic anion, dipicrylamine, carbonyl cyanide m-chlorophenylhydrazone, and NBD-phosphatidylethanolamine. Third, we demonstrate that large Ca transients can strongly enhance the extracellular binding of several membrane probes, monitored electrically or optically, consistent with a more disordered membrane with more amphipath-binding sites. Fluorescence shifts of ANEPPDHQ report increased disorder of the extracellular monolayer after large Ca transients, consistent with an increased propensity of the membrane to phase separate and vesiculate. Collectively, the results indicate that >50% of the outer monolayer is ordered and can be selectively internalized during MEND responses initiated by two very different cell perturbations.

The Journal of General Physiology

INTRODUCTION

In two companion papers (see Lariccia et al. in the January 2011 issue and Fine et al. in this issue), multiple experimental protocols are described to induce massive endocytosis (MEND) in baby hamster kidney (BHK) fibroblasts, HEK293 cells, and cardiomyocytes by apparently disparate pathways. On the one hand, large cytoplasmic Ca transients induce MEND via both short- and long-term mechanisms. On the other hand, extracellular sphingomyelinases, detergents, and amphipathic compounds cause MEND by perturbing the outer plasmalemma monolayer in the absence of Ca transients. Apart from the unprecedented magnitude of these responses, the most evident commonality of these endocytic events is that classical endocytic proteins, such as clathrin, dynamins, and actin cytoskeleton, do not appear to be involved.

To what extent MEND responses are mechanistically related to endocytosis in secretory cells is not yet clear. The actions of Ca to promote MEND in fibroblasts are not critically dependent on the canonical Ca-activated phosphatases, verified repeatedly to activate compensatory endocytosis in secretory cells (Artalejo et al., 1996; Engisch and Nowycky, 1998; Marks and McMahon, 1998; Chan and Smith, 2001; Wu et al., 2009). Furthermore, Ca-activated MEND is strongly dependent on the presence of relatively labile plasmalemmal cholesterol, being blocked by short treatments with cholesterol-chelating agents and being highly activated by cholesterol enrichment of the plasmalemma (Lariccia et al., 2011). Equivalent effects of manipulating cholesterol are not described for endocytosis in secretory cells, a complication being that mechanisms leading to exocytosis are cholesterol dependent (Wasser et al., 2007; Geumann et al., 2009).

Correspondence to Donald W. Hilgemann: donald.hilgemann@utsouthwestern.edu

Abbreviations used in this paper: BHK, baby hamster kidney; C4TPP, butyltriphenylphosphonium; C6TPP, hexyltriphenylphosphonium; C10TPP, decyltriphenylphosphonium; C12TPP, dodecyltriphenylphosphonium; CCCP, carbonyl cyanide m-chlorophenylhydrazone; DPA, dipicrylamine; DSF, diffusional security factor; DTDP, ditridecylphthalate; EDA, ethylenediamine; HPCD, hydroxypropyl-β-cyclodextrin; MEND, massive endocytosis; NBD-PE, NBD-phosphatidylethanolamine; NFA, niflumic acid; TPP, triphenylphosphonium; TtPP, tetraphenylphosphonium; TX100, Triton X-100.

The Rockefeller University Press $30.00
J. Gen. Physiol. Vol. 137 No. 2 155–172
www.jgp.org/cgi/doi/10.1085/jgp.201010470

Nonioinic detergents induce MEND at concentrations >100-fold less than those used to isolate detergent-resistant membranes. Apparently, the outer monolayer reorganizes to form lipid domains that spontaneously vesiculate inwardly, thereby fractionating the membrane in vivo and suggesting comparisons to biochemical membrane fractionation (Fine et al., 2011). Clearly, amphipath-driven MEND provides new opportunities to understand the function of lipid rafts in intact cells and their relationships to biochemically isolated detergent-resistant membrane domains (Brown, 2006; Lingwood and Simons, 2007). Because Ca-activated MEND is cholesterol dependent and does not involve classical endocytic proteins, the suspicion is raised that Ca-activated MEND occurs by mechanisms that are related to amphipath-activated MEND.

With this background, we describe here experiments that interrogate the relationships between amphipath- and Ca-activated MEND, the potential roles of lipid domains in MEND responses, and the potential use of several membrane probes to study the underlying mechanisms. We establish first that Ca transients strongly facilitate amphipath-activated MEND and that common hydrophobic compounds in the modern environment, phthalate plasticizers, can promote Ca-activated MEND. Next, we address whether internalized membrane indeed consists primarily of lipids and proteins that form *Lo* membrane domains. We provide evidence that many amphipathic membrane probes do not interact well with the membrane that is internalized. Only one probe tested here, the fluorescent dye FM 4–64, populates domains that internalize equally well as domains that remain at the cell surface, and no probe preferentially binds to domains that internalize. Thus, Ca-activated and amphipath-activated MEND indeed internalize membrane that primarily contains ordered lipid in its outer monolayer. The results provide further evidence that lipidic forces can drive physiological endocytic processes, although the identity of physiological MEND-promoting lipids remains to be established.

MATERIALS AND METHODS

BHK cell maintenance and electrical methods were as described in our companion papers (Fine et al., 2011; Lariccia et al., 2011). Solution velocities were at least 3 mm/s in experiments without imaging and ∼1 mm/s in experiments with imaging. Confocal imaging was performed as described previously (Lariccia et al., 2011), with a microscope (TE2000-U; Nikon) and a 60× 1.45 NA oil-immersion objective (Nikon). A 40-mW 163-CO_2 laser (Newport Corporation) was used for 488-nm excitation (i.e., for Bodipy, NBD, and di-4-ANEPPDHQ [ANEPPDHQ] FM dye). Time-lapse images were recorded either at 160 × 160 or 256 × 256 resolution with an ∼400–800-ms total exposure time. The routine exposure interval was 3 s. However, when fluorophore lability was evident (e.g., with NBD) imaging settings, frequency and experiment durations were adjusted to ensure that photobleaching was negligible. Lasers were operated at 4% power, with a detector pinhole setting of 100 µm and an average linear gain of 6.50. For 1-anilinonaphthalene-8-sulfonic acid (1,8 ANS), excitation was with a 175-W light source (Lambda DG-5 Xenon; Sutter Instrument Co.) with filters (Chroma Technology Corp.) set for excitation at 403/12 nm and emission at 460/40 nm. Data were collected using a camera (CoolSnap HQ; Photometrics) and analyzed using Meta Imaging Series 6.1.

Solutions and materials

The solutions used minimized all currents other than NCX1 current. Free Mg of all cytoplasmic solutions was 0.4 mM. The standard extracellular solution contained (in mM): 120 LiOH, 4 $MgCl_2$ or 2 $MgCl_2$ plus 2 $CaCl_2$, 20 TEA-OH, 10 HEPES, and 0.5 EGTA, pH 7.0 with aspartate. The standard cytoplasmic solution contained (in mM): 80 LiOH, 20 TEAOH, 15 HEPES, 40 NaOH, 0.5 $MgCl_2$, 0.5 EGTA, and 0.25 $CaCl_2$, at pH 7.0 with aspartate. Unless indicated otherwise, 0.2 mM GTP was used in nucleotide-containing solutions. All lipids were dissolved in ethanol at concentrations of 0.1–1 mM, aliquoted in light-protected vials, and stored at −30°C. 1,2-distearoyl-sn-glycero-3-phosphoethanolamine-*N*-(7-nitro-2-1,3-benzoxadiazol-4-yl) was from Avanti Polar Lipids, Inc. (18:0 NBD PE). 1,2-Dipalmitoyl-sn-glycero-3-phosphoethanolamine-*N*-(7-nitro-2-1,3-benzoxadiazol-4-yl) was from Sigma-Aldrich (16:0 NBD PE). *N*-(4,4-difluoro-5,7-dimethyl-4-bora-3a,4a-diaza-s-indacene-3-pentanoyl)sphingosyl 1-β-D-lactoside (C5 Bodipy Lactosylceramide) and Bodipy FL C5-ganglioside GM1 were from Invitrogen. 1,8 ANS was from Sigma-Aldrich. ANEPPDHQ was provided by L. Loew (University of Connecticut, Farmington, CT). Dipicrylamine (DPA; Sigma-Aldrich) was provided by W.L. Hubbell (University of California, Las Angeles, Los Angeles, CA). Ditridecylphthalate (DTDP) was provided by Exxon Mobile Corporation.

Minimal description of the function of hydrophobic ions

We use hydrophobic anions and cations in this study to detect changes of membrane properties. Previous work (Andersen and Fuchs, 1975; Bruner, 1975; Benz et al., 1976; Pickar and Brown, 1983) provides a firm basis to understand their function in membranes, including biological membranes (Chanda et al., 2005). DPA was used previously as a novel means to "amplify" capacitive signals associated with exocytosis (Oberhauser and Fernandez, 1995). As illustrated in Fig. 1 A, hydrophobic anions, such as tetraphenylborate and DPA, bind with high affinity beneath phospholipid head groups of the membrane. They translocate reversibly across 70–80% of the membrane electrical field at rates 100–10,000-fold greater than they dissociate from membranes, and as a result, they increase the effective membrane capacitance (Andersen and Fuchs, 1975). For DPA, translocation rates are in the range of 10,000–30,000 per second (Lu et al., 1995). In conventional whole cell voltage clamp, therefore, DPA-capacitive signals occur with the time constant of voltage clamp (0.2–2 ms). Hydrophobic cations (see lower cartoon in Fig. 1 A), such as tetraphenylphosphonium (TtPP) and triphenylphosphoniums (TPPs), bind to the membrane with lower affinity and generate current by translocating slowly across the membrane electrical field. These different patterns form the primary evidence for a large positive dipole potential in the interior of the membrane that promotes the binding of hydrophobic anions while hindering the binding and translocation of hydrophobic cations (Flewelling and Hubbell, 1986).

Analysis of hydrophobic anion function in bilayers reveals a complex translocation process (Andersen and Fuchs, 1975). Nevertheless, here it is adequate for us to assume that hydrophobic ions exist as two populations in the membrane. They bind and dissociate in a nearly voltage-independent fashion, and they translocate across electrical field over a single barrier,

$$dX_o / dt = X_{out} \bullet k_{ao} + X_i \bullet K_b - X_o \bullet (k_{do} + k_f) \quad (1)$$

$$dX_i / dt = X_{in} \bullet k_{ai} + X_o \bullet K_f - X_i \bullet (k_{di} + k_b), \quad (2)$$

where X_o and X_i are the amounts of hydrophobic ion associated with the outer and inner monolayers, and X_{out} and X_{in} are the free concentrations of hydrophobic ion outside and inside the cell. In the absence of a membrane electrical field, k_{ao} and k_{ai} are the respective association constants, k_{do} and k_{di} are the respective dissociation constants, and k_f and k_b are the translocation rates from out-to-in and in-to-out, respectively. In constructing a model, voltage-dependent terms must be included to modify each of the constants so that the binding, translocation, and dissociation reactions move an ion through the entire membrane field. For DPA, translocation reactions reflect ~75% of electrical field. The fraction of membrane-bound anions on the cytoplasmic side (F_i) can therefore be approximated as

$$F_i = 1 / \left(1 + e^{(E50 - Em) \bullet 0.75 \bullet F/RT}\right), \quad (3)$$

where E_{50} is the midpoint of the charge–voltage relationship. In cells used here, the E_{50} ranges from −10 to −50 mV (see Figs. 6 and S1), implying that DPA has a higher affinity for the cytoplasmic versus the extracellular leaflet of the bilayer. Analytical solutions of Eqs. 1–3 are given in the supplemental text with simplifying assumptions. For DPA, it is assumed that translocation

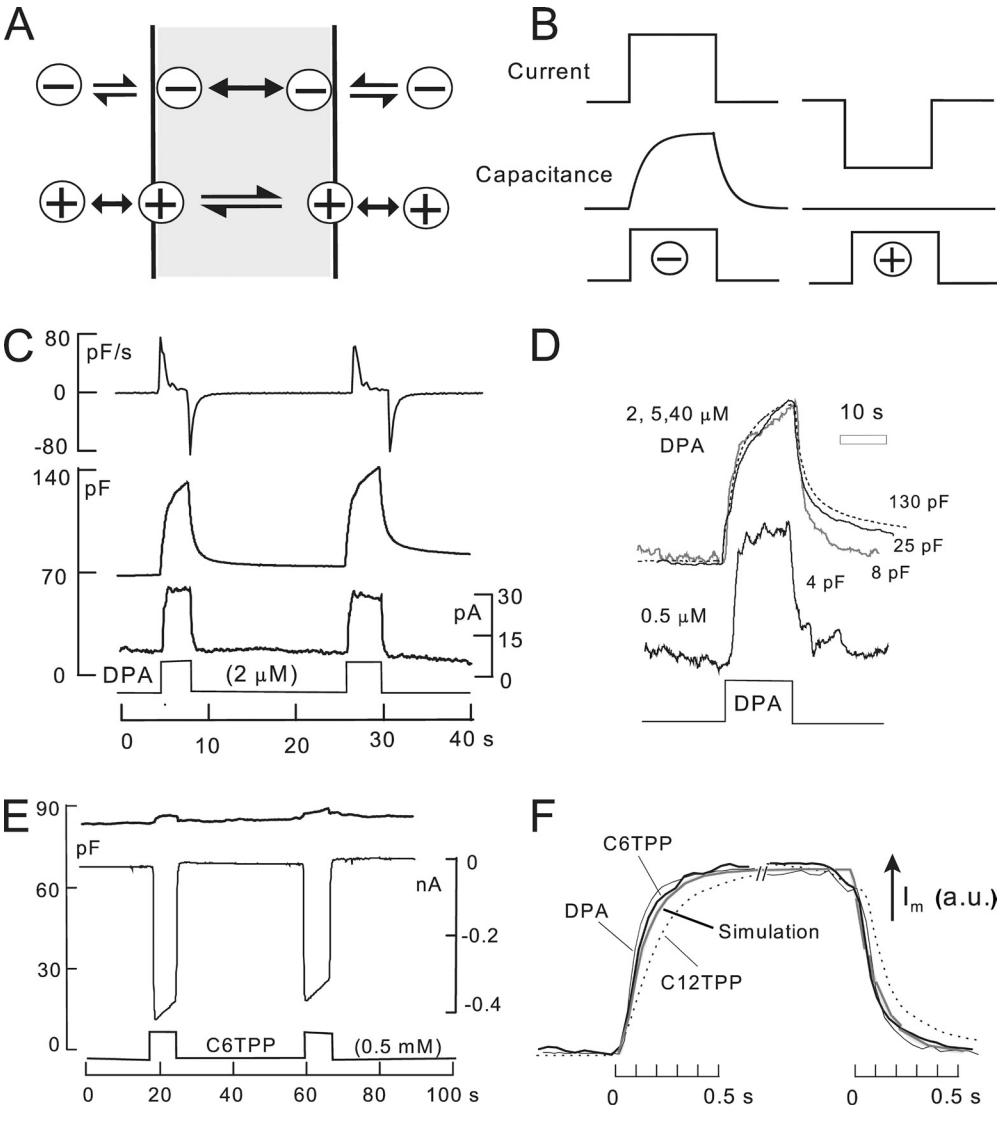

Figure 1. The function of hydrophobic anions and cations. (A) Hydrophobic anions translocate reversibly through the hydrophobic core of the membrane much faster than they dissociate from the membrane. Hydrophobic cations translocate slowly across the membrane in relation to their dissociation rates from the membrane. A positive dipole potential within the membrane is assumed to promote anion binding over cation binding by several hundredfold. (B) Predictions of simple models of hydrophobic ion function. When applied rapidly to membranes, hydrophobic anions give rise to a capacitive signal that develops with the time course of their binding/dissociation from the membrane. The net current generated by their passage through the membrane field ("flux") develops immediately. In contrast, hydrophobic cations do not generate a capacitive signal. (C) DPA-capacitive signals and currents in BHK cells using standard solutions with 2 mM ATP and 0.2 mM GTP on the cytoplasmic side. Rapid application and removal of 2 μM DPA causes an immediate outward current and a slowly rising capacitive signal, which decays toward an increased baseline upon DPA removal. The major time constant of the rising and falling signals is 0.35 s. The DSF, i.e., the ratio of minimum diffusional flux to current, is 1.8. (D) DPA-capacitive signals upon applying and removing different DPA concentrations in the same BHK cell. The signals are scaled to allow comparison of the wave forms. With low DPA concentrations, capacitive signals come to a steady state more rapidly than with high concentrations (>2 μM), and slowly decaying signal components become more pronounced with high DPA concentrations. (E) Currents and capacitance records for the application and removal of the hydrophobic cation, C6TPP (0.5 mM). Capacitance changes are negligible in relation to those evoked by DPA. (F) Normalized current records showing the time courses of current activation and deactivation upon applying and removing 2 μM DPA, 0.5 mM C6TPP, and 25 μM C12TPP. The gray curve shows the expected time course for diffusion through a 10-μm solution layer, with a diffusion coefficient of 0.5×10^{-5} cm^2/s.

reactions are instantaneous with respect to dissociation rates. For TPPs with low membrane affinity, it is assumed that binding/dissociation reactions reach a steady state instantly.

DPA current occurs as a step function with changes of DPA concentration, as illustrated in the left panel of Fig. 1 B, if the dissociation rates on the extracellular and cytoplasmic sides are equal. If dissociation is faster at the outer membrane surface than at the inner surface, current declines partially upon applying DPA, and an inward current transient develops upon removing DPA. If dissociation is faster on the cytoplasmic side, current shows an asymptotic increase upon applying DPA and an exponential declining phase upon removing DPA. As further illustrated in the left panel of Fig. 1 B, DPA-capacitive signals develop and decline to a steady state in proportion to DPA accumulated in the membrane. This time course is determined by the dissociation constants and the distribution of DPA across the membrane (i.e., $F_i \cdot k_{di} + (1-Fi) \cdot k_{do}$). As illustrated in the right panel of Fig. 1 B, the simplifying assumptions for TPPs give rise to an immediate inward current and no capacitive signal.

Relevant to several experimental results, we point out that in the simple models, the unidirectional TPP flux from outside to inside does not depend on the dissociation rate on the cytoplasmic side. A decrease of dissociation rates on both membrane sides increases TPP influx by increasing the affinity on the outside. The same changes have no effect on DPA current but increase capacitive signals by promoting DPA partitioning into the membrane.

Fig. 1 C shows DPA signals recorded in BHK cells at 22°C. On fast application and removal of 2 µM DPA at 0 mV, a small steady outward membrane current turns on and off as rapidly as the cell can be manually switched between solution streams. C_m rises and falls approximately exponentially with time constants on the order of 0.5 s. However, the final return of C_m to baseline is slow, reflecting accumulation of DPA within the cell. The top record in Fig. 1 C is the first derivative of the capacitance record. From the initial rate of rise of C_m (~80 pF/s) and the slope of the DPA charge–voltage relation at 0 mV (i.e., Eq. 3 with $E_{50} = -30$ mV; $dF_o/dEm \approx 6/V$), one can estimate the initial current required to build up the charge associated with the capacitance. In Fig. 1 C, the DPA flux calculated from the capacitance signal amounts to 80 pF/s/6, i.e., 13 pA. Notably, the calculated flux is substantially smaller than the DPA current per se, which amounts to 22 pA. At 37°C, this discrepancy was routinely about threefold and often fourfold. Thus, the buildup of charge in the membrane and the DPA current measured are not well coupled. The explanation appears to be that a large part of the DPA current is generated by a mechanism different from the capacitive signals. First, as described in Fig. S2, DPA currents usually decrease substantially at lower temperatures, whereas capacitive signals change very little. Second, as evident in several results presented (e.g., Figs. 9 A, S3, and S4), DPA currents change very little when DPA-capacitive signals change by severalfold.

Fig. 1 D shows DPA-capacitive signals obtained for the application and removal of four different DPA concentrations in the same BHK cell. For concentrations of 2–40 µM, the rising DPA signals can be scaled reasonably, but the falling signals reveal slowly decaying components at higher concentrations. For lower DPA concentrations, i.e., <2 µM, capacitive signals reach a near steady state more rapidly than with higher concentrations.

Fig. 1 E shows representative electrical signals for TPPs. In this example, 0.5 mM hexyltriphenylphosphonium (C6TPP) is applied and removed twice. In contrast to DPA, capacitive signals are negligible, and large inward currents (approximately −0.4 nA) develop and decay with solution changes, as expected from the simple model. Over 2–4 s, these currents typically decay by 5–15%. The time courses of current activation and deactivation are shown in better detail in Fig. 1 F, whereby records of DPA, C6TPP, and dodecyltriphenylphosphonium (C12TPP) currents are scaled to one another. For DPA and C6TPP, as well as other short-chain TPPs, currents reach 63% of steady state within 120 ms. As apparent in Fig. 1 F, this time course was routinely longer for C12TPP.

The time courses of current activation and deactivation for DPA and C6TPP signals may reflect the mechanics of solution switches, diffusion through immobile water layers at the cell surface, or initial binding reactions at the cell surface. For the C12TPP signals, we describe in Fig. S2 that these time courses are strongly temperature sensitive and therefore probably reflect binding/dissociation reactions. We describe in Fig. S3 that concentration–absorbance relations for TtPP and C12TPP give no evidence for aggregation or micelle formation.

Assuming that time courses for DPA and C6TPP reflect diffusion through unstirred water layers at the cell surface, the maximal distances over which diffusion can be taking place are readily determined from diffusion simulations. The gray curve in Fig. 1 F represents the time course of diffusion across a 10-µm-thick water layer with a diffusion coefficient of 0.5×10^{-5} cm^2/s, as expected for molecules with molecular weights of 400–550. The rising and falling DPA and C6TPP currents are routinely as rapid, or more rapid, than this time course. As described next, these potential constraints allow us to calculate for each experiment a minimum flux that will be supported by diffusion.

Two potential pitfalls: diffusion limitations and the disposition of DPA in experimental solutions

Physical limitations of diffusion up to the cell surface can potentially limit hydrophobic ion fluxes, and concern is greatest for DPA because it is used in concentrations of only 2 or 3 µM. Although we routinely observe a rapid flow of particles directly past cells, we cannot prove that the mechanics of solution changes determine the time course of current changes in these experiments. Therefore, we calculate for each experiment the minimum flux that can be supported by diffusion via Fick's law. As demonstrated in Fig. 1 F, current time courses in response to concentration jumps indicate that maximal diffusional distances are 10 µm. The relevant area for the calculation is that of a sphere with the diameter of the cell, which corresponds to the cell surface area after strong MEND. When MEND is not activated in an experiment, the relevant area is assumed to be 40% of cell area. We assume a diffusion coefficient of 0.5×10^{-5} cm^2/s and that 1 pF represents 100 µm^2 of membrane. Diffusional fluxes, converted to picoampere equivalents, can then be related to measured fluxes and expressed as a ratio. In the text and figures of this paper, we refer to the ratio of the minimal flux supported by diffusion to the measured hydrophobic ion current as a diffusional security factor (DSF):

$$DSF = Flux_{max} / Flux_{real}, \quad (4)$$

where $Flux_{max}$ is the minimal flux supported by diffusion, and $Flux_{real}$ is the current generated by the hydrophobic ion of interest. A DFS of 1 indicates that the measured flux may be strongly limited by diffusion. As described in Results, DSF calculations for TPPs raise concern only for C12TPP, and this concern is subsequently alleviated by five lines of experimentation. The DSF for C6TPP (0.5 mM) in Fig. 1 E is 50, effectively eliminating a role for diffusion restriction in currents generated.

The DSF for DPA in Fig. 1 C is 3.6, indicating that diffusion might significantly limit DPA flux into cells. Therefore, we formally deemphasize results dependent on DPA fluxes in our presentation, but still point out the best argument against diffusion limitation: DPA flux into the cell membrane (i.e., $\Delta pF/\Delta t$) increased by a factor of 2 after Ca transients (Fig. 9), by a factor of 3–10 during cholesterol extraction (Fig. S11), and by a factor

of 3 with membrane fluidizers (Fig. S12). This would not be possible if DPA fluxes were substantively limited by diffusion. Steady-state measurements of DPA-capacitive signals, with DPA on both membrane sides, to be presented, are diffusion independent and support the same conclusions suggested by unidirectional fluxes.

Finally, we point out that DPA, like functionally similar oxonols (Plásek and Sigler, 1996), aggregates over time in experimental solutions. At concentrations of 2–20 µM, precipitation in experimental solutions is readily monitored as a loss of absorbance, with halftimes of 15–20 min. To effectively hinder precipitation, DMSO must be used in the range of 20 volume percent, and we have chosen to work with maximally 2% DMSO. Furthermore, DPA and/or DPA precipitates bind to the Teflon solution lines used in our experiments. As a result, free DPA concentrations become dependent on flow rate, whereby a step increase of flow unleashes DPA from the tubing walls. For these reasons, DPA solutions were prepared freshly before each experiment, and solution flow rates were carefully controlled. With these precautions, 10–20 DPA consecutive responses were highly reproducible over experimental times of >20 min. For the hydrophobic cations, similar issues have not arisen. As described for two cations in Fig. S5, concentration–absorbance relations are linear up to the millimolar range. The functional activities of TPP solutions were indefinitely stable.

Online supplemental material

Analytical solutions for the simple model of hydrophobic ion function described in Materials and methods are presented in the supplemental text. Fig. S1 demonstrates that Ca transients associated with exocytosis strongly increase DPA-capacitive signals during continuous DPA application, without a significant change of the DPA capacitance–voltage relation. Fig. S2 demonstrates that DPA currents are usually strongly temperature dependent, whereas DPA-capacitive signals are not. Figs. S3 and S4 show that β-cyclodextrin treatments and benzyl alcohol strongly increase DPA-capacitive signals, whereas DPA currents increase only a little or not at all. Fig. S5 shows that concentration–absorbance relations for C12TPP and TtPP are linear over the concentration range of micromolar to the millimolar. Fig. S6 illustrates that a low concentration of NP-40 promotes Ca/high ATP-dependent MEND. Fig. S7 shows that Ca transients associated with exocytosis strongly promote cyclodextrin-induced loss of cell capacitance and the formation of channels by the phosphatidylethanolamine-binding antibiotic, duramycin. Fig. S8 demonstrates that C12TPP currents are strongly reduced by lowering temperature, without affecting their insensitivity to MEND. Fig. S9 shows that decyltriphenylphosphonium (C10TPP) currents are similarly temperature sensitive and are nearly unaffected by MEND at low temperature. Thus, insensitivity to MEND cannot be explained by diffusion limitation of TPP currents. Fig. S10 shows that C12TPP does not induce MEND from the cytoplasmic side. Fig. S11 shows that MEND is associated with larger decreases of C6TPP currents at high versus low C6TPP concentrations. Figs. S12–S14 document that DPA-capacitive signals decrease less than C_m during all Ca-activated MEND protocols. Fig. S15 shows that extended treatment of cells with β-cyclodextrans can increase DPA-capacitive binding signals by more than one log unit, and Fig. S16 shows that C6TPP currents and capacitive signals are also increased severalfold by cyclodextran treatment. Fig. S17 documents that ANEPPDHQ binding to BHK cells, determined optically, is unaffected by Ca/ATP-dependent MEND, and Fig. S18 demonstrates that capacitive binding signals for ANEPPDHQ are unaffected by MEND, whereas FM 4–64 signals are strongly decreased. The online supplemental material is available at http://www.jgp.org/cgi/content/full/jgp.201010470/DC1.

RESULTS

First, experimental results are presented that demonstrate functional coupling between amphipath- and Ca-activated MEND. Second, electrophysiological evidence is presented that both forms of MEND internalize membrane that does not bind well multiple electrogenic membrane probes. Third, we present data demonstrating that Ca transients, which do not immediately cause MEND, can strongly enhance the binding of electrogenic membrane probes. Finally, we present equivalent experiments for fluorescent membrane probes.

Amphipaths can mimic cholesterol in promoting MEND

Amphipathic compounds at low concentrations make cholesterol more available for oxidation by cholesterol oxidase and for extraction by cyclodextrins by binding in the membrane in a manner that is partially competitive with cholesterol (Lange et al., 2009). Thus, there is functional coupling between amphipaths and cholesterol. As described in our companion paper (Lariccia et al., 2011), cholesterol enrichment does not cause MEND under basal cell conditions. However, it strongly promotes Ca-activated MEND and effectively induces MEND after Ca transients subside, even several minutes thereafter. Fig. 2 documents these same properties for amphipathic compounds.

Fig. 2 illustrates our routine observation that Ca transients causing exocytosis reduce the threshold concentrations of amphipathic compounds that cause MEND. The experiment described in Fig. 2 A (>20 observations) uses a BHK cell with an ATP-free cytoplasmic solution. Initially, Triton X-100 (TX100) is without effect at a concentration of 80 µM, applied and removed twice for periods of 40 and 25 s. The activation of Ca influx by NCX1 for 15 s causes a 25% increase of C_m that, as usual in the absence of ATP, is stable over the duration of an experiment. Thereafter, the same detergent-containing solution that was without effect causes a rapid 50% MEND response. Fig. 2 B illustrates the same result for the anti-neoplastic alkyl-lyso lipid, edelfosine (van der Luit et al., 2007). A 25-µM concentration of edelfosine has no evident effect before a Ca influx episode. After a Ca influx episode, however, the same edelfosine-containing solution induces a MEND response amounting to >60% of the cell surface.

Fig. 2 C presents results for an amphipath that has no discernable effect before evoking a Ca transient, but then causes MEND in conjunction with the Ca transient (20 similar observations). The amphipath is a plasticizer, DTDP, which has splayed alkyl chains. Thus, DTDP presumably interacts differently with membranes than with detergents. DTDP is negligibly soluble in aqueous solutions (see material safety data sheet). The extracellular solution used in Fig. 2 C contains 5 µM DTDP, prepared by sonication, and the cytoplasmic solution contains

no ATP, GTP, or polyamines. The DTDP-containing solution has no discernable effect on C_m before activating a Ca transient, but Ca influx then causes MEND within seconds, similar to cholesterol enrichment (Lariccia et al., 2011).

On the basis of these results, we conclude that the long-lived action of Ca to promote MEND (Lariccia et al., 2011) extends to amphipathic agents. In Fig. S6, the facilitation of Ca-activated MEND by the presence of a low concentration of NP-40 is illustrated. In Fig. S7, it is demonstrated that the ability of cyclodextrins to decrease

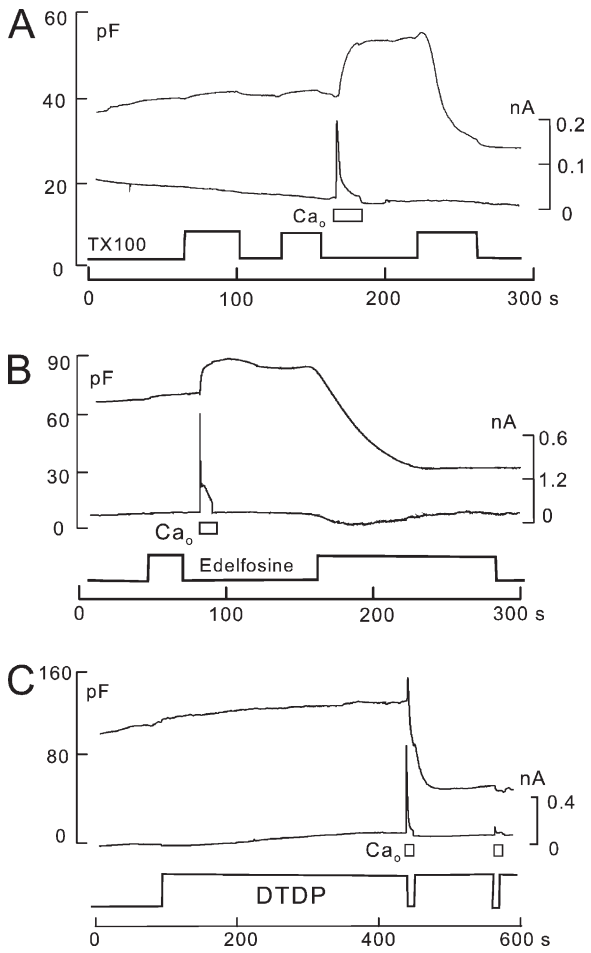

Figure 2. Amphipath-induced MEND is facilitated by Ca transients associated with exocytosis. Cytoplasmic solutions are ATP and GTP free. (A) As with many other amphipaths that induce MEND, the threshold concentrations needed to induce MEND by TX100 are reduced by a Ca transient associated with exocytosis. In this example, 80 µM TX100 was applied twice before the activation of Ca influx, and it was without effect. After Ca influx and exocytosis, the same TX100 concentration causes a rapid 50% MEND response. (B) Similar to TX100, a low concentration of edelfosine (30 µM) is without effect before the activation of Ca influx. After a Ca influx episode, the same edelfosine concentration causes a 65% MEND response. (C) DTDP-saturated extracellular solution (5 µM; sonicated for 5 min) is without effect when applied for 5 min before the activation of reverse Na/Ca exchange. Subsequent activation of Ca influx by NCX1 causes a rapid 60% MEND response.

C_m by extraction of lipids is greatly enhanced by Ca transients, and it is demonstrated that the ability of a phosphatidylethanolamine-binding antibiotic, duramycin, to form ion-conducting channels (Navarro et al., 1985) in BHK cells is greatly enhanced after Ca transients. Collectively, these results suggest that large cytoplasmic Ca transients trigger mechanisms that modify the extracellular plasmalemma monolayer.

Insensitivity of electrogenic membrane probes to MEND

Next, we document that membrane internalized in both amphipath- and Ca-induced MEND binds a variety of membrane probes relatively weakly. Figs. 3 and 4 describe results for amphipath-induced MEND, and Figs. 5–8 describe results for Ca-activated MEND.

Fig. 3 A describes MEND induced by the hydrophobic cation, C12TPP, which is also a detergent. Because C12TPP is a hydrophobic cation, it translocates across the membrane and thereby generates an inward current during its application. Using standard solutions (Lariccia et al., 2011) with 2 mM ATP, C12TPP induces MEND in the concentration range of 20–50 µM. Although other alkane detergents, SDS and dodecylglucoside (Fine et al., 2011), cause MEND only when they are removed from the extracellular side, C12TPP (40 µM in Fig. 3 A) induces MEND during its application to the outer cell surface. As apparent in the current record (lower record in Fig. 3 A), C12TPP generates a 0.16-nA inward current during the 10 s required to cause MEND that amounts to 65% of the cell surface. After inducing MEND, a second application of C12TPP causes an inward current of nearly the same magnitude. Even the partial current decay that occurs over time is similar before and after MEND.

As illustrated in the inset of Fig. 3 A, steady-state current–voltage relations for C12TPP were determined in five experiments by applying and removing C12TPP at multiple membrane potentials. Under the conditions of these experiments, current saturates with hyperpolarization, raising a concern that currents might be limited by diffusion. The following results speak against this possibility. First, the DSF for the experiment in Fig. 3 A, as well as for four equivalent experiments, is 6.6. Second, as shown in Fig. S8 A, C12TPP currents are strongly temperature dependent, as are their activation/deactivation time courses. Thus, the saturation of current with hyperpolarization probably reflects slow association kinetics of C12TPP with the outer plasmalemma monolayer. Third, as described in Fig. S8 B, when C12TPP currents are recorded at 18°C, versus 37°C, currents are reduced more than threefold, but TX100-induced MEND does not cause a reduction of the C12TPP current. Fourth, as shown in Figs. 3 C and S9, currents generated by the C10 analogue of C12TPP, C10TPP, are also nearly unaffected by TX100-induced MEND, although DSF values are nearly a log unit higher. Fifth, as shown in

Fig. S9, steady-state current–voltage relations for C10TPP are steep at 15°C, although the currents are not reduced by TX100-induced MEND. Thus, diffusion cannot be limiting. We conclude that C12TPP and C10TPP bind at least five times more effectively to membrane that remains at the cell surface than to membrane that is internalized in TX100-induced MEND.

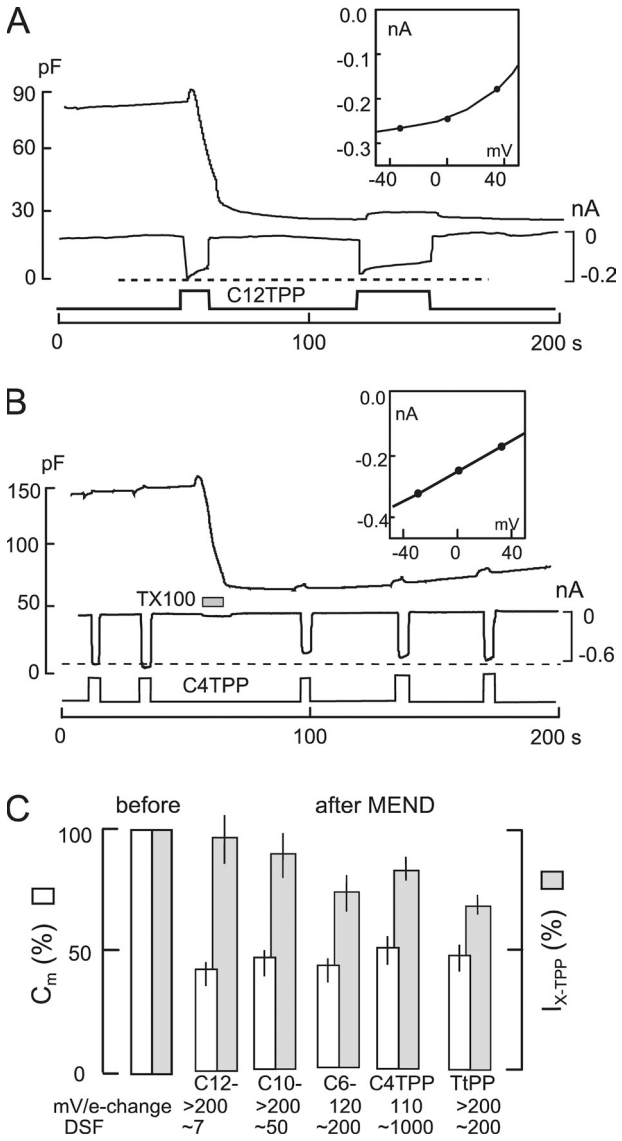

Figure 3. Insensitivity of TPP currents to MEND. BHK cells using standard solutions with 2 mM ATP and 0.2 mM GTP on the cytoplasmic side. (A) The rapid application of extracellular solution containing 40 µM C12TPP causes an immediate 0.2-nA inward current and a MEND response amounting to 70% of C_m within 15 s. Thereafter, the renewed application of C12TPP generates an inward current of similar magnitude but no further loss of C_m. DSF, 6.6. (B) The rapid application of 10 mM C4TPP induces an inward current of 0.6 nA. After the induction of a 63% MEND response with 200 µM TX100, the C4TPP current is reduced by only 12% on average. DSF, 1,017. (C) Normalized results ($n = 5$) for the same protocols using 40 µM C12TPP, 0.12 mM C10TPP, 0.25 mM C6TPP, 10 mM C4TPP, and 0.5 mM TtPP. The average MEND responses ranged from 45 to 57%. The average current decrease was 10% for C12TPP, 15% for C10TPP, 26% for C6TPP, 17% for C4TPP, and 31% for TtPP. Slopes of current–voltage relations and average DSP values are given below the bar graphs for each agent.

Finally, in relation to Fig. 3 A, we note that the total cytoplasmic C12TPP concentration reaches ∼100 µM, as calculated from cell dimension and current magnitudes. Nevertheless, almost no outward current is generated upon removing C12TPP. Presumably, C12TPP that enters cells is mostly bound by membranes and constituents of the cytoplasm. We demonstrate in Fig. S10 that C12TPP, like other detergents (Fine et al., 2011), does not cause MEND from the cytoplasmic side, even when perfused into cells at eight times the effective extracellular concentration.

Equivalent experiments for TPPs having shorter side chains and for TtPP are described in Fig. 3 (B and C). As the alkyl chain is decreased in length, the analogues must be used at much higher concentrations to generate equivalent currents. Fig. 3 B illustrates an experiment with 10 mM butyltriphenylphosphonium (C4TPP) in which MEND was induced by 200 µM TX100, and C4TPP currents were evaluated before and after MEND. On average, the C4TPP current amounts to −0.6 nA before and −0.54 nA after inducing a 65% MEND response. The current–voltage relation (see inset in Fig. 3 B) is about one half as steep as expected from the simple model. The DSF for the experiment is 1,017. Thus, diffusional limitations can play no role in this shape or the relative insensitivity of C4TPP to MEND.

Fig. 3 C presents the composite results for the series of TPPs and for TtPP under the same conditions. Currents generated by 40 µM C12TPP were nearly unaffected by C12TPP-induced MEND. Currents generated by 130 µM C10TPP were nearly unaffected by TX100-induced MEND, whereas currents mediated by 0.5 mM C6TPP and 10 mM C4TPP were decreased by 26 and 14%, respectively. Thus, shorter side chains may allow TPPs partial access to membrane regions that are internalized. For 0.5 mM TtPP, access appears to be still greater. TtPP currents decrease by >25% when TX100-induced MEND amounts to 50%. Thus, the affinity of TtPP for membrane that internalizes appears to be only twofold less than that for the remaining membrane.

That short TPPs may bind with low affinity to ordered membrane domains is not surprising. FM dyes, which are hydrophobic cations that do not translocate the membrane, bind rather evenly to membrane that does and does not internalize (Fine et al., 2011). Furthermore, high concentrations of short chain TPPs can cause MEND in a pattern similar to the detergent SDS (Fine et al., 2011). During the application of these compounds, C_m is stable and MEND occurs rapidly upon their wash-off. Possibly, this pattern reflects an inhibition of membrane fission by binding within the domains that subsequently internalize on wash-off. Regardless of

details, all amphipathic membrane probes may be expected to gain access to ordered membrane domains, as their concentrations are increased. Fig. S11 demonstrates that the fractional decrease of C6TPP current after TX100-induced MEND increases from 5 to 25% when the C6TPP concentration is increased from 50 μM (DSF, 32) to 1,000 μM (DSF, 158). These results underscore that preferential binding of membrane probes to domains is likely to be highly concentration dependent.

Fig. 4 A, and subsequently Fig. 7 A, demonstrates that DPA signals are also relatively insensitive to MEND induced by 200 μM TX100. The outcomes from experiment sets under different conditions range from modest sensitivity, as in Fig. 4 A, to no sensitivity. To ensure a DSF value of >4, this experiment series was performed at 22°C. Furthermore, flow rates were increased until some cell deformation was evident. 2-μM DPA signals were examined twice before and twice after inducing MEND with 200 μM TX100. A decrease of C_m by 60% is accompanied by a decrease of DPA-capacitive signals by 28%, a decrease of the DPA binding rate (i.e., dC_m/dt; Fig. 4 A, top trace) by 37%, and no change of the DPA current. DPA current increases by a factor of 2 when temperature is increased to 37°C, demonstrating that DPA current is not limited by diffusion.

Fig. 4 B presents an equivalent experiment using 10 μM of the protonophore, carbonyl cyanide m-chlorophenylhydrazone (CCCP), to induce an outward current corresponding to outward proton transport in a cell with the standard solutions set to pH 6.5 and 7.8 in the cytoplasmic and extracellular solutions, respectively. The outward CCCP current, ~200 pA, develops and dissipates rapidly and stably upon applying and removing CCCP four times before and four times after inducing MEND response with 200 μM TX100. MEND results in a 51% decrease of C_m, whereas the CCCP current is decreased by only 13%.

Fig. 4 C shows composite data for DPA and CCCP from five and six similar experiments, respectively, together with equivalent data for three additional ionophores. On average, DPA-capacitive signals decrease by 26% when C_m decreases by 50% in TX100-induced MEND, suggesting that DPA affinity for membrane that internalizes is about one half of its affinity for membrane that remains at the cell surface. The composite results for CCCP are very similar. Currents and/or conductances generated by the ionophores valinomycin (25 μM), nonactin (12 μM), and nystatin (65 μM) are presented in the additional bar graphs in Fig. 4 C. Each ionophore was applied to BHK cells for 15 s and then removed, similar to the protocols for DPA and CCCP. The conductance caused by each ionophore developed and washed out over the course of 10–40 s, similar to results in giant patches (Hilgemann and Collins, 1992). For valinomycin, solutions contained 40 mM K on both membrane sides, and cell conductance was used as an indicator of ionophore activity. MEND caused by 120 μM TX100 amounted on average to 50% of the cell surface, whereas the activities of ionophores were changed

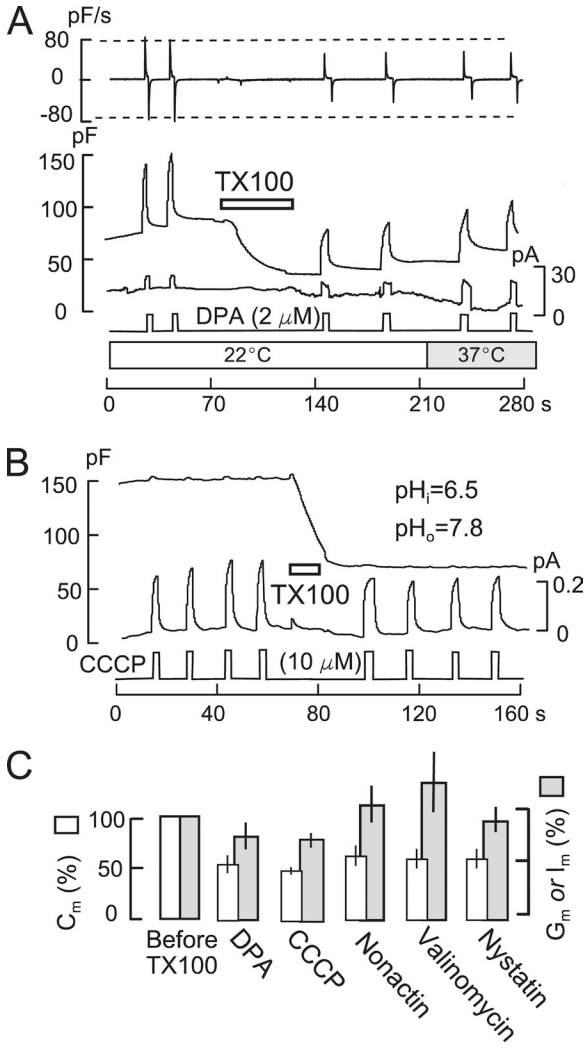

Figure 4. DPA and multiple ionophores show low sensitivity to TX100-promoted MEND. BHK cells with standard solutions containing 2 mM ATP and 0.2 mM GTP on the cytoplasmic side. (A) 2 μM DPA is applied twice before and twice after the induction of MEND by 200 μM TX100 at 22°C. DSF, 4.4. MEND amounts to 54% of C_m, whereas the capacitive DPA signals decrease by 28%. DPA currents are unchanged by MEND but double upon warming to 37°C. (B) 10 μM CCCP is applied and removed four times before and four times after inducing MEND with 200 μM TX100. To generate outward proton transport, the cytoplasmic solution was set to pH 6.5 and the extracellular solution was set to 7.8. A 51% MEND response results in a 13% decrease of the CCCP current. (C) Composite results for several electrogenic membrane probes. In all cases, TX100 causes an ~50% loss of C_m. DPA-capacitive signals ($n = 5$) and CCCP currents ($n = 6$) are decreased by 25% on average. The conductance induced by 12 μM nonactin ($n = 4$) and 25 μM valinomycin ($n = 4$) is increased on average by 15 and 27%, respectively, after TX100-induced MEND. The conductance induced by the application and removal of 65 μM nystatin ($n = 4$) is decreased by 15% ($n = 4$).

very little. Only the nystatin conductance was decreased detectably by MEND. Thus, multiple commonly used ionophores appear to associate preferentially with membrane that does not internalize.

Electrogenic membrane probes are insensitive to Ca-induced MEND

Fig. 5 presents records of Ca-activated MEND in which C6TPP currents were recorded before and after MEND with standard solutions at 37°C (10 observations). Lower temperatures were not used because the NCX1 transporter becomes strongly inhibited. To promote fast Ca-activated MEND in Fig. 5 A, the cytoplasmic solution contained 2 mM of the polyamine, ethylenediamine (EDA), together with 2 mM ATP and 0.2 mM GTP. As indicated below the C_m and current records, 300 µM C6TPP was applied and removed five times, generating an inward current ~0.3 nA in magnitude each time. After the first two C6TPP responses, reverse Na/Ca exchange current was activated by applying 2 mM Ca for 20 s. MEND occurs during Ca influx and amounts to 60% of C_m. Thereafter, the C6TPP current is decreased by only 15%. The DSF of this experiment is 70, thereby eliminating any influence of diffusion. Fig. 5 B gives composite results for five similar experiments. An average MEND response of 50% is accompanied by an average 12% decrease of C6TPP current.

Fig. 5 C presents an equivalent experiment in which high cytoplasmic ATP (8 mM) promotes progressive Ca-activated MEND without polyamines. In this experiment, Ca transients via reverse Na/Ca exchange were activated four times. Over the course of three Ca transients, separated by 2 min, 45% of the cell surface was lost. 0.3 mM C6TPP was applied and removed 10 times during the observation period. C6TPP currents did not significantly decrease during the experiment, which had a DSF of 59.

DPA signals were often nearly unaffected by Ca-induced MEND, with the potential caveat that experiments must be performed at 37°C, giving rise to relatively large DPA currents and small DSF values of 3–4. In Fig. 6, an example is presented that illustrates how DPA-capacitive signals are analyzed subsequently in the absence of DPA flux. In this experiment, the cytoplasmic solution contains 1 mM of cytoplasmic spermidine with 2 mM ATP and 0.2 mM GTP to promote

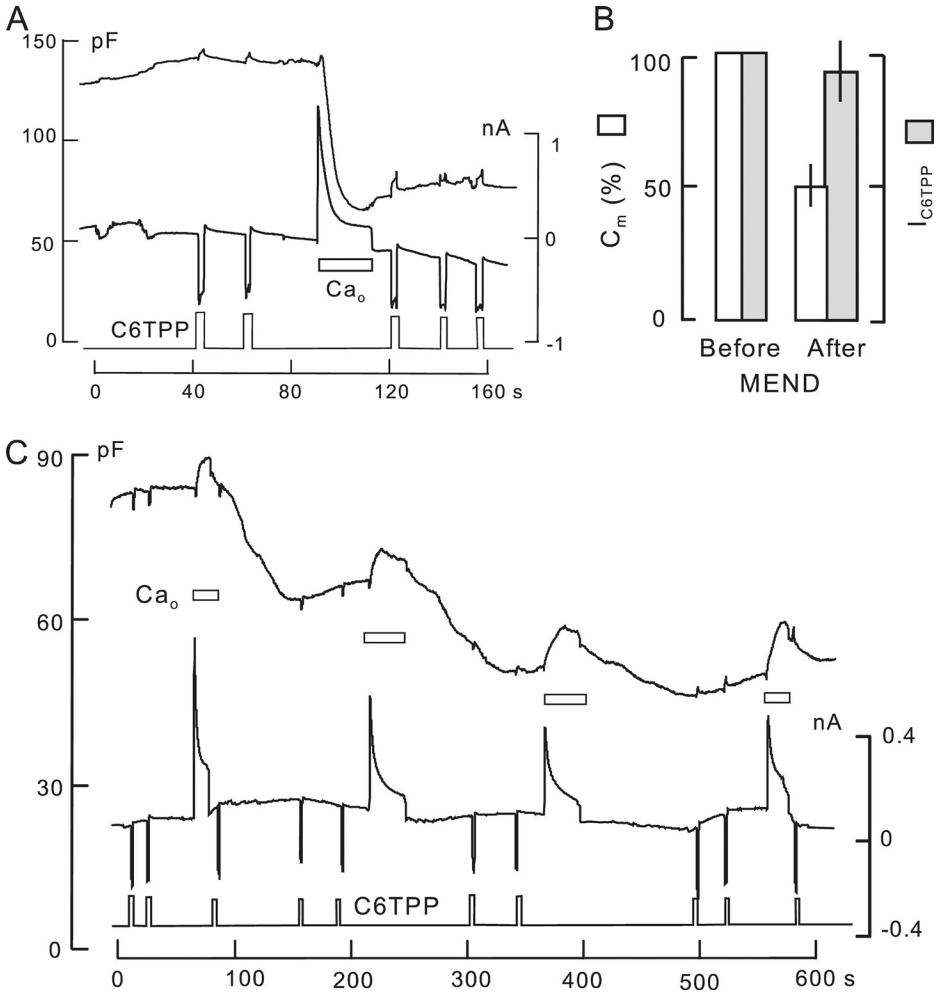

Figure 5. C6TPP currents are nearly unaffected by Ca-induced MEND. 0.3 mM C6TPP is applied briefly multiple times in each experiment, as indicated. (A) 2 mM of the polyamine, EDA, is included in both the cytoplasmic and extracellular solutions to promote rapid MEND (50% in 5 s) during Ca influx by NCX1. Thereafter, C6TPP current is decreased by 12% on average. DSF, 50. (B) Composite results for four experiments similar to A. Ca-activated MEND causes a 50% loss of C_m, whereas C12TPP currents decrease by just 10%. (C) Using a cytoplasmic solution with 6 mM ATP and no polyamine, Ca influx by NCX1 is activated four times. C_m decreases substantially in a delayed fashion after each of the Ca influx episodes, resulting finally in a 45% decrease of C_m. 0.3-mM C6TPP currents are unchanged. DSF, 41.

MEND during the Ca influx episode. As indicated, 2 μM DPA was applied and removed twice before and twice after the Ca influx episode, which caused a 61% MEND response. During each application of DPA, voltage ramps were applied to determine the C_m–voltage relationship of DPA. Fig. 6 (B and C) shows C_m records before and after MEND, together with data fits to rising and falling exponential function. Fig. 6 D shows the C_m–voltage relations for DPA from the voltage ramps, together with nearly invisible data fits to the first derivative of a Boltzmann function as dotted lines. The rising and falling signals in Fig. 2 (B and C) have time constants from 0.67 to 0.82 s, with no clear differences before and after MEND. The amplitudes and voltage midpoints of capacitance–voltage relations are only marginally changed. Thus, DPA signals are unaffected by MEND in this experiment (DSF, 3.6).

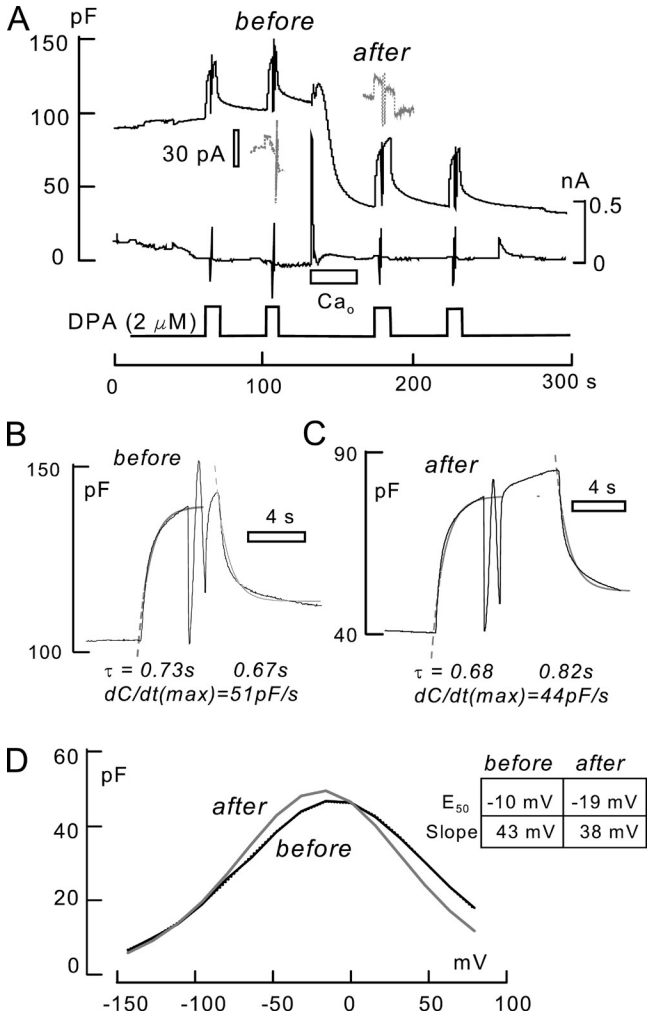

Figure 6. Analysis of DPA-capacitive signals before and after MEND induced by a Ca transient in the presence of 1 mM spermidine and 6 mM ATP. MEND amounts to 68% of C_m. DSF, 4.0. (A) 2 μM DPA is applied twice before MEND and twice after MEND for times of 6–10 s. During each application of DPA, voltage is stepped to −150 mV and then ramped to +80 mV to determine the capacitance–voltage relation of DPA. (B and C) Capacitance records indicated by "before" and "after" in A. The magnitudes of DPA-capacitive signal and the time constants of the rising and falling signals (0.67–0.82 s) are not detectably changed. (D) The magnitudes of DPA capacitance–voltage relations are not detectably changed; the peak capacitance undergoes a small 8-mV shift to more negative potentials.

Diffusion-independent DPA-capacitive signals sense MEND weakly

Next, we show that the apparent insensitivity of DPA signals to Ca-activated MEND may be exaggerated because Ca transients cause a large increase of DPA binding that counteracts the influence of MEND. As illustrated by Fig. 6 D, DPA-capacitive signals can be quantified in voltage pulse experiments without removing DPA from the cell. To do so, membrane voltage must be stepped to a potential at which the DPA-capacitive signal is negligible, and the drop of capacitance indicates the contribution of DPA to total capacitance. In this way, DPA-capacitive signals can be studied with DPA on both membrane sides, thereby minimizing any influence of DPA diffusion on experiments. Because the midpoint of the DPA capacitance–voltage relation occurs at a negative potential, we step potential to a positive potential (+120 mV) every 8 s for 1.2 s. Because positive membrane potential drives DPA from the extracellular side to the cytoplasmic side, we use a higher cytoplasmic concentration (6 μM) of DPA than extracellular concentration (2 μM). With these conditions, total cell capacitance is very stable over experimental times of 5–15 min.

Fig. 7 A shows the results of this protocol for TX100-induced MEND, and Fig. 7 B shows the results for Ca-induced MEND. Four similar experiments were obtained for each MEND type. In Fig. 7 A, 200 μM TX100 was applied twice and removed twice to induce a maximal MEND response. The decline of C_m (see dotted line) amounted to 46%. As in all experiments with this protocol, DPA-capacitive signals defined by a positive voltage pulse did not decline at all. Thus, under these conditions, DPA-capacitive signals are more insensitive to TX100-induced MEND than those shown in Fig. 4.

In Fig. 7 B, Ca influx by NCX1 was activated twice in the presence of 8 mM of cytoplasmic ATP to initiate Ca/ATP-dependent MEND. At the first Ca influx episode, the DPA-capacitive signal increased nearly fourfold in parallel with a 20% increase of C_m. This super-proportional increase of DPA capacitance is consistent with the fact that Ca transients enhance the ability of multiple amphipaths to induce MEND (Fig. 2). As described subsequently, Ca transients also strongly enhance the partitioning of other membrane probes into the membrane. After the second Ca influx episode, MEND occurring over 1 min amounts to 60% of cell capacitance. During MEND, the DPA-capacitive signal decreases from 71 to 55 pF: The 60% decrease of membrane area results in a 20% decrease of the DPA-capacitive signal. In reasonable agreement with

results for TX100 MEND in Fig. 4 A, DPA binds in these experiments with approximately threefold lower affinity to membrane that internalizes than to membrane that does not internalize.

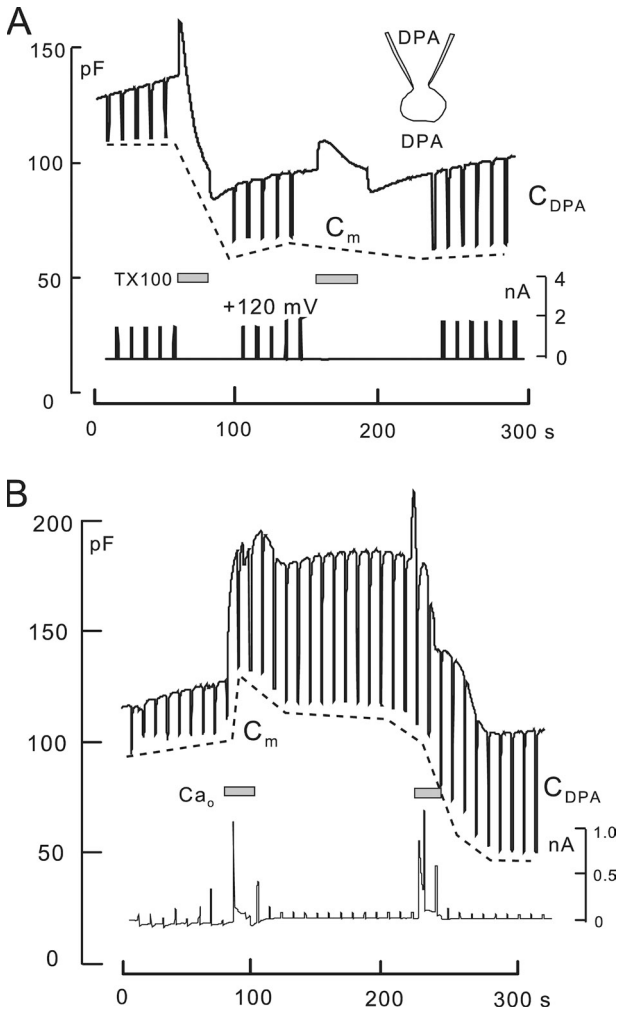

Figure 7. Steady-state DPA-capacitive signal changes in response to TX100- and Ca-induced MEND. BHK cells with standard solutions, 8 mM of cytoplasmic ATP, 2 µM extracellular DPA, and 6 µM of cytoplasmic DPA. The DPA- and membrane-related capacitance components are determined by applying voltage pulses to +120 mV for 1.3 s. Membrane capacitance does not depend on voltage, whereas the DPA capacitance becomes negligible at +120 mM. Membrane capacitance is demarcated by a dotted line. (A) TX100-induced MEND. Upon the first application of TX100, MEND amounts to just 50% of the initial cell area. The DPA-capacitive signal, defined by the downward deflections of capacitance, is unchanged by MEND. After a second application of TX100, DPA-capacitive signals increase slowly by 20% with respect to the pre-MEND magnitude. (B) Ca-induced MEND with high (8 mM) ATP and no polyamine in response to two Ca transients. The first Ca transient causes exocytosis without subsequent endocytosis. Cell capacitance increases by 20%, whereas the DPA-capacitive signal increases by nearly threefold. The second Ca transient causes little further exocytosis and a delayed MEND response amounting to 60% of the cell surface. The DPA-capacitive signal decreases in parallel by 20%.

Figs. S12–S14 present experiments that examine DPA signal changes, with each Ca-activated MEND protocol described previously (Lariccia et al., 2011). Fig. 8 gives the average normalized membrane capacitance (C_m), DPA currents (I_{DPA}), and DPA-capacitive signals (C_{DPA}) from three experiments for each protocol. All DPA signals are normalized to magnitudes before the indicated events (Fig. 8; leftmost bars, 100%). From left to right, the second set of bars shows that Ca influx by NCX1 caused on average a 25% increase of C_m in cells that did not undergo immediate MEND (i.e., cells without ATP). The increase of C_m was accompanied by a threefold greater increase of DPA capacitance and a 25% increase of DPA current. When high ATP (8 mM) was included in cytoplasmic solutions (Fig. 8, third group of bars), promoting delayed MEND, the DPA-capacitive signals and DPA currents reversed on average to baseline, whereas cell capacitance decreased to 50% below baseline. These results are consistent with experiments just outlined: DPA must bind to membrane that internalizes with two- to threefold lower affinity than to membrane that remains at the cell surface. In response to Ca influx in the presence of polyamines (Fig. 8, fourth set of bars), both DPA currents and capacitive signals remain on average increased after >50% of cell area is lost.

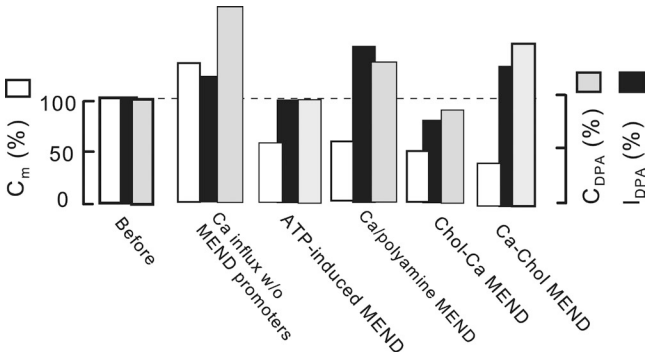

Figure 8. Summary of changes of DPA signals in response to a single Ca influx episode and multiple Ca-dependent MEND protocols. Examples of each experiment type are presented in Figs. S12–S14. Each bar set gives give the average of three or more experiments for cell capacitance, DPA capacitance, and DPA currents, normalized to their initial experimental values (leftmost bar set). From left to right, Ca influx causes on average a threefold greater increase of DPA capacitance than cell capacitance, and a small increase of DPA current. After Ca influx, the presence of high ATP in the cytoplasm causes a return of DPA capacitance and current to baseline, whereas cell capacitance decreased to 50% below baseline. Polyamine/Ca-induced MEND causes on average an increase of DPA capacitance and current, whereas cell capacitance decreases to 55% below baseline. When cells are enriched with cholesterol, Ca influx without polyamines causes a 58% decrease of cell capacitance, whereas DPA capacitance and current decrease on averaged by 18 and 15%. Cholesterol enrichment after a Ca transient has increased cell capacitance by 25% results on average in a decrease of cell capacitance by 66%, whereas DPA capacitance and current remain 18 and 25% greater than baseline.

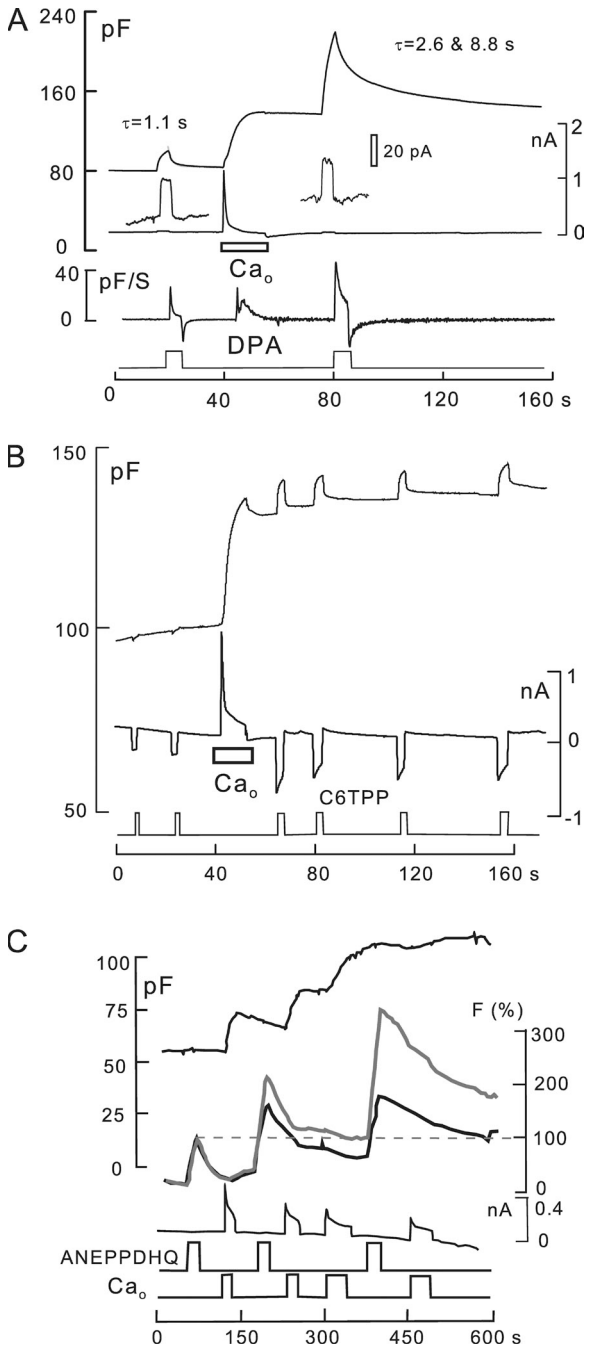

Figure 9. Ca transients associated with exocytosis cause dramatic changes of the surface membrane, as reported by electrogenic and optical membrane probes. Standard solutions with no ATP or polyamines. (A) Effects on DPA signals. 2 µM DPA was applied for 4 s and removed before and after activating reverse Na/Ca exchange in the absence of cytoplasmic ATP. C_m increases by 60%, and the DPA-capacitive signal increases by a factor of 4. The DPA current is unchanged, whereas the rate of rise of the capacitive DPA signal (dC_m/dt, measured in pF/S) is increased by 70%. DSP, 3.3. (B) Effects on C6TPP signals. 300 µM C6TPP is applied and removed six times. Ca influx associated with a 40% increase of membrane area causes a 2.4-fold increase of C6TPP currents, causes decay phases of the currents, and induces C6TPP to develop a capacitive signal component. These changes are consistent with decreased dissociation rates from the membrane, similar to the effects of DPA. DSF, 670. (C) Effects on ANEPPDHQ optical signals. Ca transients with membrane fusion cause large shifts in fluorescence spectra of ANEPPDHQ (8 µM) binding. The large relative increase of emission above 640 nm (gray line) is similar to changes described for cholesterol depletion and presumably increased membrane disorder (Jin et al., 2006). Electrophysiological parameters were recorded in parallel with time-lapse confocal imaging at emission bandwidths of 500–580 nm (black) and 640 nmLP (gray).

This increase reflects with good certainty the long-term effect of Ca on the outer monolayer. Similarly, Ca influx after cholesterol loading with hydroxypropyl-β-cyclodextrin (HPCD)–cholesterol complexes causes, overall, three- to fourfold smaller reductions of DPA signals than reductions of cell area. When cholesterol is enriched after a Ca transient, cholesterol-induced MEND causes a 70% loss of cell area, with only a 15% loss of DPA-capacitive signal. In this case, the membrane internalized (i.e., cholesterol-enriched membrane) evidently has a fivefold lower affinity for DPA than membrane remaining at the cell surface. This outcome is consistent with Fig. S15, which demonstrates that cholesterol extraction can increase the affinity of the plasmalemma for DPA by at least one log unit.

Ca transients cause increased membrane disorder that is sensed by multiple membrane probes

As described above, DPA-capacitive signals are strongly increased by large Ca transients, and Fig. 9 A demonstrates that DPA binding rates are increased, whereas DPA dissociation rates are decreased. In this experiment, 2 µM DPA was applied for 5 s and removed before and after a Ca influx episode in the absence of cytoplasmic nucleotides. C_m increases by 66% during the Ca transient and is stable after Ca influx is terminated. Although the DSF of the experiment is only 2.2, the rate of rise of DPA capacitance (i.e., dC_m/dt; Fig. 9 A, top trace) is nearly doubled after the Ca transient (>20 similar observations). The magnitude of the capacitive DPA signal is increased 3.5-fold, and it decays more slowly upon the removal of DPA. Although decay of the DPA signal before fusion is reasonably described by one exponential function (τ = 1.1 s), two exponentials are required after membrane fusion (τ = 2.6 and 8.8 s). In summary, Ca transients strongly increase partitioning of DPA into the membrane, as expected for DPA binding in a more disordered membrane (Smejtek and Wang, 1990). In Figs. S3, S4, and S15, we show that β-cyclodextrins and a fluidizing agent strongly increase DPA binding, consistent with signal changes in Fig. 9 A reflecting increased membrane disorder.

Fig. 9 B shows the equivalent changes of C6TPP signals (0.3 mM) routinely observed in response to Ca transients under the same conditions. In contrast to DPA, the C6TPP current increases by more than twofold

when membrane area increases by only 30%. As noted in Materials and methods, a decrease of dissociation rates on both membrane sides will increase C6TPP currents but not DPA currents. After the Ca influx episode, capacitive signals become evident upon applying and removing C6TPP (20 observations). In Fig. S16, we describe that β-cyclodextran treatments cause very similar changes of C6TPP currents, consistent with signals in Fig. 9 reflecting increased disorder.

As described in Fig. 9 C, results for the styryl dye ANEPPDHQ document further that Ca transients cause increased disorder in the outer monolayer. This dye undergoes large fluorescence shifts in cholesterol-rich versus cholesterol-poor membranes (Jin et al., 2006). As indicated in Fig. 9 C, 8 µM ANEPPDHQ was applied and removed multiple times before and after activating Ca influx multiples times in cells with no cytoplasmic nucleotides. Fluorescence was monitored in a bandwidth of 500–580 nm (black) and above 640 nm (gray). In response to multiple Ca influx episodes, C_m increases by twofold, and ANEPPDHQ fluorescence increases over-proportionally. The long wavelength component (640LP) and its rate of rise increase by threefold, whereas the shorter wavelength component (500–580) increases only 30%, as would be expected for increased disorder (Jin et al., 2006).

Other anionic membrane probes: niflumic acid (NFA) does not sense MEND

Because DPA gains partial access to the membrane that internalizes in MEND, we tested whether other anionic membrane probes might bind more specifically to either the membrane fraction that internalizes or does not internalize. Among the probes tested, the chloride channel blocker, NFA (Hogg et al., 1994), was notable because it generates a large capacitive binding signal that does not involve translocation of charge across the bilayer. As described in Fig. 10, NFA binding to the outer monolayer is insensitive to MEND.

Fig. 10 A illustrates the capacitive binding signal generated by the rapid application and removal of 0.2 mM NFA using a BHK cell with standard solutions with 2 mM ATP and 0.2 mM GTP. C_m increases monotonically by ~13% upon applying NFA and recedes toward baseline in two distinct phases upon its removal. As with detergents, the capacitance signal may reflect lateral expansion and thinning of the membrane. Because the magnitude of the NFA signal is unusually large, however, it cannot be excluded that NFA enters partially into the membrane's electrical field. As shown in Fig. 10 B, the NFA-capacitive binding signal is only weakly voltage dependent. Fig. 10 (C and D) demonstrates that the capacitive binding signal of NFA is unaffected by

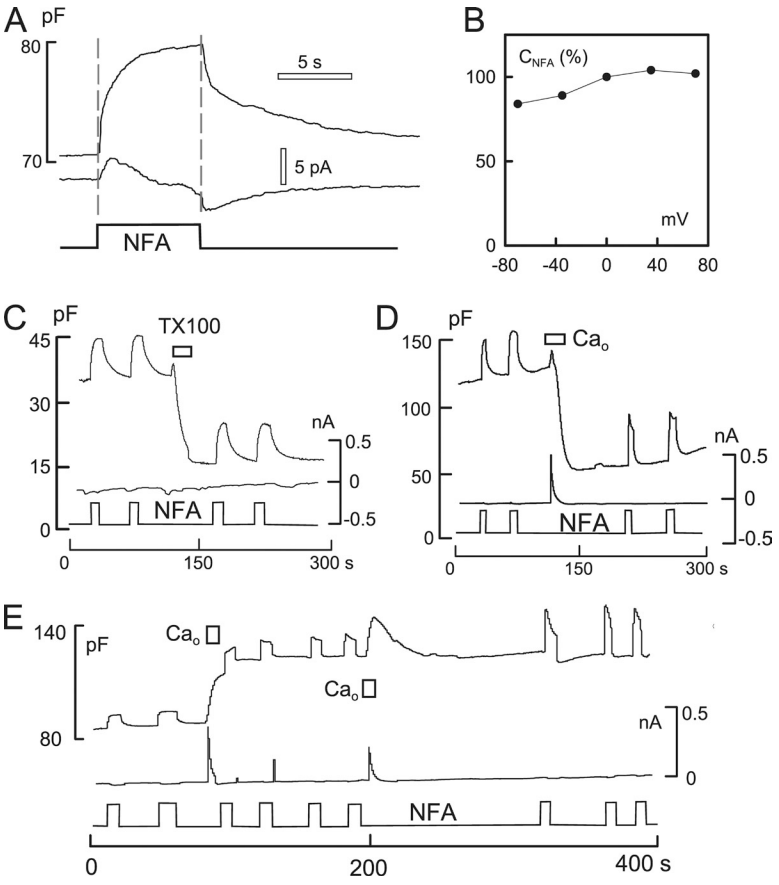

Figure 10. Capacitive binding signals for the hydrophobic Cl^- channel blocker, NFA (0.2 mM), are nearly unchanged by MEND. BHK cells with standard solutions. (A) The application and removal of NFA causes a robust increase of C_m. Decay of the C_m signal occurs in two distinct phases. Currents associated with NFA application are very small, or absent, and show a delay from the onset of the rise of C_m. (B) The capacitance–voltage relation of the NFA signal is nearly flat, indicating that capacitive signals do not arise from translocation of the probe across the membrane. (C) The capacitive signal induced by NFA is unaffected by TX100-induced MEND. (D) MEND induced by Ca influx in the presence of 2 mM EDA in both cytoplasmic and extracellular solutions. The capacitive signal induced by NFA rises and falls faster after Ca-induced MEND, but its magnitude is not affected. (E) Effect of Ca influx associated with exocytosis without MEND on NFA-capacitive signals. Cytoplasmic solutions contain no ATP and no polyamine. The Ca transient results in a 60% increase of C_m and a smaller increase of the NFA signal. After a second Ca transient, the NFA signal is nearly doubled and becomes faster.

TX100-induced MEND and Ca-induced MEND in the presence of polyamine (EDA; 2 mM on both membrane sides), respectively. As shown in Fig. 10 E, NFA signals increase roughly in proportion to cell capacitance when Ca influx causes exocytosis without subsequent endocytosis (i.e., without cytoplasmic nucleotides or polyamines). The NFA signal can then be further increased by subsequent Ca transients, although membrane area does not increase.

Most optical membrane probes sense MEND only weakly

In contrast to ANEPPDHQ fluorescence changes in response to Ca transients (Fig. 9 C), Fig. 11 demonstrates that the binding rates and spectral properties of ANEPPDHQ dye are nearly unchanged by MEND, caused either by TX100 or Ca influx. Fig. 11 A illustrates an experiment monitoring ANEPPDHQ fluorescence before and after TX100-induced MEND, as well as its potential uptake during MEND. 8 µM of ANEPPDHQ dye was applied and removed multiple times to establish its binding-dissociation characteristics. As demonstrated by the micrographs, the cell membrane labeled and unlabeled consistently with the application and removal of dye. During the second application of dye, 150 µM TX100 was applied together with dye for 10 s, resulting in MEND that amounts to >70% of the cell surface. After wash-out of dye for 25 s, the residual fluorescence is only 10% higher than before MEND (Fig. 11 A, gray lines). The lack of dye retention is in complete disparity to the large MEND response. Furthermore, upon applying dye again after MEND, it is evident that the rate of dye binding is nearly unchanged.

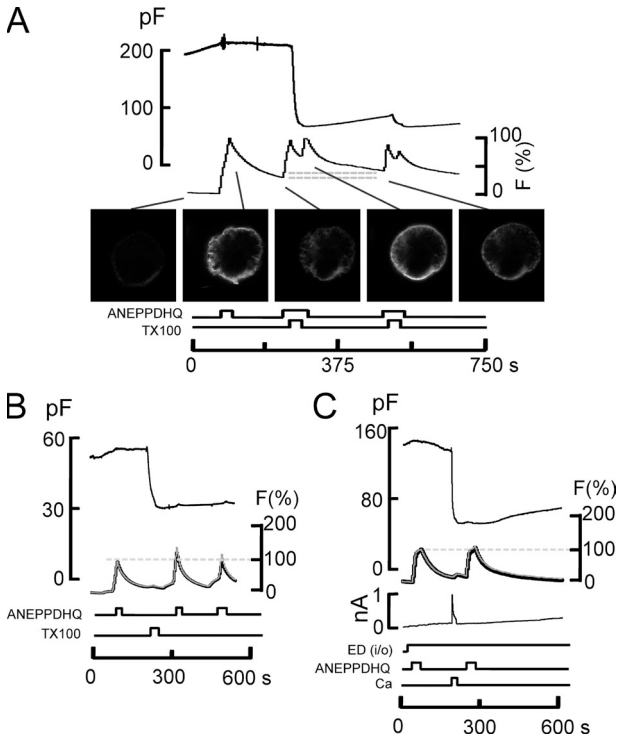

Figure 11. The styryl dye, ANEPPDHQ, does not occupy the membrane that internalizes during TX100- and Ca-activated MEND in BHK cells. (A) 10 µM ANEPPDHQ was applied before MEND and removed during the induction of MEND with 150 µM TX100 and again after MEND. The apparent binding rates of ANEPPDHQ are unchanged by the removal of >70% of the cell surface by MEND, and the amount of fluorescence internalized during MEND (i.e., does not wash off) amounts to no more than 15% of the initial labeling (see horizontal gray lines). (B) 8 µM ANEPPDHQ was applied and removed before and after TX100 (150 µM)–induced MEND while imaging at bandwidths of 500–580 nm (black) and 640 nmLP (gray). The optical records are scaled. Neither the apparent binding rates of ANEPPDHQ nor its spectral properties are changed after TX100-induced MEND. (C) Same as B, using Ca influx in the presence of polyamine, here EDA, to induce MEND. Dye signals, which approach a steady state in these records, are unchanged by MEND.

In experiments presented in Fig. 11 (B and C), ANEPPDHQ fluorescence was monitored in two wavelength bands, as in Fig. 9 C, before and after inducing MEND with 180 µM TX100. MEND results in no spectral shifts of the dye, and the apparent rates of dye binding are unchanged by MEND. We stress that in Fig. 11 C, dye loading comes nearly to a steady state. Thus, limitations of dye access to the membrane, i.e., diffusional limitations, cannot explain the failure of MEND to affect dye loading. Similar results for Ca-activated MEND that is ATP dependent are presented in Fig. S17. We conclude that, in contrast to FM dyes (Fine et al., 2011), ANEPPDHQ does not associate well with the membrane that is internalized during MEND (i.e., >50% of the cell surface). As expected from these optical results, Fig. S18 shows that the capacitive binding signal of ANEPPDHQ does not decrease with MEND, whereas the capacitive binding signal of FM 4–64 does decrease.

Fig. 12 documents that other fluorescent membrane probes are also largely excluded from domains that are internalized during MEND, whereas a head group–labeled phosphatidylethanolamine (C16/18 NBD-phosphatidylethanolamine [NBD-PE]) shows an intermediate behavior. Similar to experiments shown in Fig. 11, fluorescently labeled lipids and membrane dyes were applied and removed from BHK cells multiple times before and after MEND was induced by 150 µM TX100. Their binding rates, assumed to be proportional to the rate of rise of fluorescence, are related to capacitance loss by TX100-induced MEND. Several classes of lipids and probes were used. As shown in Fig. 12 A, a short-chain ganglioside, C5-GM1, labeled with Bodipy, traditionally a marker for glycosphingolipid-enriched rafts, binds at the same rates before and after the induction of a 50% MEND response by TX100. Unlike FM 4–64, the Bodipy GM1 probe washes off only very slowly. As shown subsequently, however, the difference in dissociation rates cannot explain why the binding of C5-GM1 is unchanged by MEND. We note that in multiple experiments, the wash-off rates of this dye became greater after MEND.

Head group–labeled NBD-PE is an optical probe that might preferentially associate with ordered membrane because of its straight side chains and relatively small head group. Although the effective use of this probe is limited by its low solubility, we could establish conditions with 10% DMSO that generated consistent, homogeneous labeling of cells. Using 5 µM NBD-PE, Fig. 12 B shows that NBD-PE labeling is indeed reduced in rate after TX100-induced MEND. However, its binding is clearly not preferentially decreased.

Fig. 12 C shows composite results for most fluorescent probes used. The binding rate of FM 4–64 decreases nearly in proportion to membrane area. The binding of the probe 1-anilinonaphthalene-8-sulfonic acid, at concentrations of 100–300 µM, decreased by 20% on average, with MEND responses amounting to 50% of the cell surface on average. The NBD-PE probe showed intermediate sensitivity to MEND, with the average percent decrease of NBD-PE binding being about one half the average percent decrease of membrane area in response to MEND. Probes that were insensitive to MEND include ANEPPDHQ, C5-bodipy GM1, and C5-lactosylceramide.

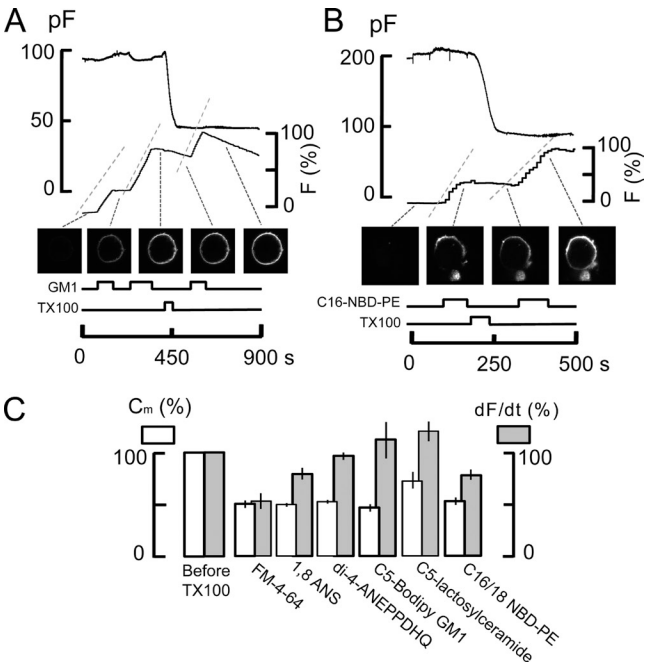

Figure 12. Optically determined binding rates of multiple lipid probes in BHK cells before and after inducing MEND with 150 µM TX100. Binding rates of dyes are assumed to be proportional to the rate of fluorescence increase over 20 s upon applying dyes. The gray dashed lines alongside of the fluorescence records indicate the average rate of fluorescence increase. (A) An experiment using 1 µM C5-Bodipy-Gm1. (B) An experiment using 5 µM C16:0-NBD-PE in the presence of 10% DMSO to promote lipid solubility. (C) Summary of results showing capacitance loss in white and binding rates of fluorescent probes in gray. Only the styryl FM dye and the C16:0-NBD-PE are significantly affected by TX100-induced MEND.

DISCUSSION

Multiple electrogenic and optical membrane probes have been used to analyze changes of the physical properties of the plasma membrane in cells undergoing large endocytic responses (MEND). Massive internalization of membrane, caused by Ca transients or amphipathic compounds, leave the binding and/or activities of several membrane probes relatively unaffected. In contrast, Ca transients that do not trigger endocytosis cause membrane changes that strongly promote the binding of many membrane probes (e.g., Figs. 8, 9, 10, S1, S7, and S12), and this increased binding can reverse partially during subsequent endocytosis. Except for FM dyes, however, signals from membrane probes decrease proportionally much less than cell area during endocytic responses analyzed in this paper.

These results together provide a new line of evidence for the existence of lipid domains in living cells (Lingwood and Simons, 2010). The results suggest that >50% of the outer monolayer is ordered, and they suggest an order of affinities for diverse membrane probes in *Lo* versus *Ld* membrane domains (Fig. 13), discussed subsequently. Most importantly, the results provide support for a profound functional role of lipid domains. Cells can potentially regulate large endocytic responses by relatively small modifications of the membrane lipid composition, with endocytosis being driven by lipidic forces.

The long-term mechanism by which Ca promotes amphipath-activated MEND

In our companion paper by Lariccia et al. (2011), we show that a large Ca transient enables ATP, phosphatidylinositiol-bis 4,5-phosphate, cholesterol, and a second Ca transient to subsequently cause MEND. Here, these observations are extended to amphipathic compounds, namely TX100, eldelfosine, and DTDP (Fig. 2). These compounds all cause MEND at lower concentrations after a Ca transient than before the Ca transient. Ca transients act as if they generate more binding sites for these amphipathic agents, and this functional interpretation is physically verified by hydrophobic ion signals as well as by optical signals. The binding of DPA and ANEPPDHQ increases severalfold more than membrane area in response to a Ca transient (Figs. 7 B and 9). Hydrophobic cation currents are similarly facilitated, and the fluorescence spectrum of ANEPPDHQ shifts as expected for a more disordered membrane (Fig. 9 C). In addition, β-methylcyclodextrin extracts cholesterol and phospholipids more readily, and the phosphatidylethanolamine-binding antibiotic, duramycin, generates ion channels more readily after a Ca influx episode (Fig. S7).

Two interpretations are possible. The entire extracellular monolayer may exist in a relatively ordered state that becomes disrupted by processes associated with Ca transients with the new generation of disordered domains. Alternatively, the outer monolayer transitions from a more

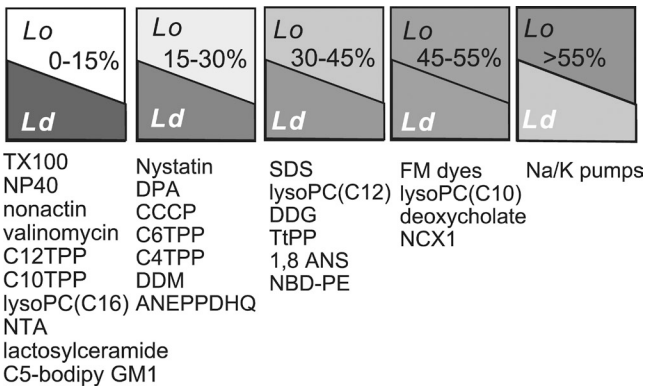

Figure 13. Summary of membrane probes studied in this paper and our companion paper by Fine et al. (2011) in relation to MEND responses. The figure represents best estimates of their distribution between membrane domains that internalize and those that do not internalize during MEND, interpreted to represent *Lo* and *Ld* domains, respectively. From left to right, the group with the highest relative affinity for disordered membrane is the largest group. It includes nonionic detergents, carrier-type ionophores, long-chain TPPs, NFA, and lactosylceramide. The second group, which is modestly affected by MEND, includes nystatin, DPA, CCCP, short-chain TPPs, dodecylmaltoside (DDM), and ANEPPDHQ. The third group, which is substantially but still under-proportionally affected by MEND, includes SDS, dodecylglucoside (DDG), TtPP, 1-anilinonaphthalene-8-sulfonic acid (1,8 ANS), and NBD-PE. Similar to TPPs, lyso-PCs appear to associate more effectively with membrane that internalizes as the carbon chain length is decreased. FM dyes, deoxychoate, and NCX1 are affected proportionally by MEND, or nearly proportionally. From all probes and transporters examined to date, only Na/K pump activities are preferentially reduced by MEND, with the implication that pumps may be regulated by *Lo* domain–dependent endocytosis.

homogeneous state to a more phase-separated state in which disordered regions become more disordered and ordered regions become more ordered. The second explanation is more consistent with the most current hypotheses about membrane ordering (Lingwood and Simons, 2010). To prove this, however, membrane probes will be required that can report more specifically the state of ordered versus disordered membrane domains.

Ordered domains in the plasmalemma are thought to be substantially smaller than required to form a vesicle (Edidin, 2003; de Almeida et al., 2005; Kenworthy, 2005; Lingwood and Simons, 2010). Because 50–70% of the outer monolayer can be internalized during MEND, with little effect on several membrane probes, the more ordered membrane domains must constitute at least one half of the cell surface. This estimate is only marginally greater than some previous estimates (e.g., Gidwani et al., 2001), and it begs the idea that ordered domains form an interconnected patchwork. Contact points between ordered domains may represent points of pending coalescence. As we suggested previously (Fine et al., 2011), internalization of ordered membrane requires that disordered domains form "caps" and ordered domains segregate into valleys.

The differential sensitivities of membrane probes to MEND

Datasets for electrogenic probes, fluorescent membrane probes, and other amphipaths that generate capacitive signals give a consistent picture (see Fig. 13). The binding of the majority of probes is affected relatively weakly by MEND, or not at all, independent of MEND type. From >20 small molecule amphipaths that we have examined by electrical and/or optical measurements, no probe was found to bind selectively to membrane that internalizes. In two cases, both optical and electrophysiological signals could be analyzed and were found to be in good agreement. The capacitive binding signal for ANEPPDHQ does not decrease with MEND, similar to optical signals, whereas the capacitive binding signal for FM 4–64 does decrease, similar to optical signals (Fig. S18).

In the TPP series (Fig. 3), C12 and C10 alkyl chains hinder association with the membrane that internalizes compared with C6 and C4 chains. The strongest apparent association with internalizing membrane is obtained when the alkyl chain is replaced by a phenyl group in TtPP. A similar principle holds for FM dyes compared with the structurally similar ANEPPDHQ dye. ANEPPDHQ, which does not bind well to membrane that internalizes, has longer side chains and a bulkier hydrophobic core than FM dyes. The hydrophobic anion, NFA, is small, similar to FM dyes, but it has in contrast little or no access to membrane that internalizes (Fig. 10). Thus, charge may play a role in the segregation of membrane probes to domains. From the probes used, cationic amphipaths that do not penetrate deeply have the best apparent access to ordered membrane domains. A potential caveat in this conclusion is that electrogenic membrane probes would be expected to show MEND sensitivity if they preferentially translocate between monolayers at the interface between domains.

For multiple reasons, DPA appeared to be a promising probe to analyze membrane heterogeneity in relation to MEND. Dissociation of DPA from membranes shows multiple components, DPA binding and dissociation are highly cholesterol and Ca dependent (Figs. S1, S3, and S15), DPA naturally interrogates both membrane monolayers, and DPA can be used as a voltage-gated fluorescence quencher (Chanda et al., 2005). After substantial efforts, however, the utility of DPA for the goals of this paper appears limited. Its partitioning into disordered membrane is not selective enough to be a reliable probe for disordered membrane. Depending on the experimental protocol, the apparent partitioning of DPA to membrane that internalizes is as high as 30% or <10% (Fig. 4 A vs. Fig. 7 B, and Fig. 6 vs. Fig. 7 B). Its translocation rates, which may well be different in *Lo* versus *Ld* membrane regions, or in interfacial regions, are too rapid to measure in whole cell voltage clamp, and the DPA-generated current is enigmatic. Finally, diffusional limitations cannot be discounted when DPA flux is occurring (e.g., Fig. 6). Equivalent

probes with lower membrane affinity and lower translocation rates would be highly advantageous, and oxonols are the obvious candidates for future efforts (Plásek and Sigler, 1996).

Most of the optical probes used here have been used in studies of artificial membranes in ordered and/or gel states versus disordered states. Several results suggest that *Lo* domains in cells used here are more ordered than *Lo* phases in simple model membranes that develop phase separations. The dye, ANEPPDHQ, which senses ordered versus disordered domains in artificial membranes (Jin et al., 2006), is not able to occupy the cell surface that internalizes with MEND. In a simple two-phospholipid system, the NBD-PE used here partitions into ordered phases with twofold preference (Mesquita et al., 2000). In our experiments, NBD-PE binding decreases by 22% on average when 50% of the cell surface internalizes (Fig. 12 C). Thus, the affinity of this probe for membrane that remains at the cell surface is about twofold higher than for membrane that internalizes. Its relative preference for ordered versus disordered membrane is reversed from the two-component membrane, perhaps reflecting the increased order imposed by a high cholesterol content in the BHK cell membrane.

Lactosylceramide is used to follow uptake of membrane via caveolae-based endocytosis (Sharma et al., 2005). That its uptake is little affected by MEND underscores that MEND does not represent internalization of caveolae. The bodipy-GM1 probe would generally be expected to incorporate into membrane domains that participate in endocytosis with cholera toxin, the best-defined lipid-based sorting pathway to date. It is not significantly internalized during MEND. Consistent with our results, it has recently been shown that the raft domains into which GM1 segregates are distinct, and necessarily smaller, than the overall *Lo* phase of cell membranes (Kaiser et al., 2009).

As noted already, only FM 4–64 reports quantitatively a loss of membrane equivalent to C_m changes during MEND (Fine et al., 2011), and the capacitive binding signal of FM 4–64 decreases with MEND (Fig. S18). In our view, the identification of membrane probes that can bind more selectively to *Lo* domains are a prerequisite for progress in understanding the role of *Lo* domain–dependent endocytosis in cells. An ideal probe would bind and unbind quickly, could be monitored by both optical and electrical methods, and would not hinder fission of *Lo* domains.

In summary, Ca- and amphipath-activated MEND appear to share a common lipidic basis: the reorganization of lipid domains in a manner in which *Lo* membrane domains become internalized. That amphipaths effectively induce MEND at relatively low temperatures (Figs. S8 and S9) is consistent with membrane phase transitions (e.g., Levental et al., 2009) playing a key role, as opposed to complex biochemical processes. Possibly, MEND represents an evolutionarily primitive form of endocytosis that developed in parallel with lipid metabolism. Its high sensitivity to lipid composition may have both pharmacological and toxicological implications. That Ca-activated MEND can be promoted with high affinity by a phthalate plasticizer (Fig. 2 C) might be relevant to phthalate toxicity to the immune system (Shigeno et al., 2009). More relevant to this study, phthalates or related amphipaths may be useful to manipulate Ca-activated MEND and thereby better define its roles in physiological cell functions.

We express heartfelt gratitude to Dr. Olaf S. Andersen (Weill Medical College, New York, NY) for criticism, advice, discussions, and encouragement.

This work was supported by grants RO1-HL067942 and RO1-HL513223 to D.W. Hilgemann. We thank Mei-Jung Lin for technical assistance and Dr. Leslie M. Loew (University of Connecticut, Farmington, CT) for the generous gift of ANNEPPDHQ.

Edward N. Pugh Jr. served as editor.

Submitted: 3 May 2010
Accepted: 21 December 2010

REFERENCES

Andersen, P.S., and M. Fuchs. 1975. Potential energy barriers to ion transport within lipid bilayers. Studies with tetraphenylborate. *Biophys. J.* 15:795–830. doi:10.1016/S0006-3495(75)85856-5

Artalejo, C.R., A. Elhamdani, and H.C. Palfrey. 1996. Calmodulin is the divalent cation receptor for rapid endocytosis, but not exocytosis, in adrenal chromaffin cells. *Neuron.* 16:195–205. doi:10.1016/S0896-6273(00)80036-7

Benz, R., P. Läuger, and K. Janko. 1976. Transport kinetics of hydrophobic ions in lipid bilayer membranes. Charge-pulse relaxation studies. *Biochim. Biophys. Acta.* 455:701–720. doi:10.1016/0005-2736(76)90042-0

Brown, D.A. 2006. Lipid rafts, detergent-resistant membranes, and raft targeting signals. *Physiology (Bethesda).* 21:430–439.

Bruner, L.J. 1975. The interaction of hydrophobic ions with lipid bilayer membranes. *J. Membr. Biol.* 22:125–141. doi:10.1007/BF01868167

Chan, S.A., and C. Smith. 2001. Physiological stimuli evoke two forms of endocytosis in bovine chromaffin cells. *J. Physiol.* 537:871–885. doi:10.1113/jphysiol.2001.012838

Chanda, B., R. Blunck, L.C. Faria, F.E. Schweizer, I. Mody, and F. Bezanilla. 2005. A hybrid approach to measuring electrical activity in genetically specified neurons. *Nat. Neurosci.* 8:1619–1626. doi:10.1038/nn1558

de Almeida, R.F., L.M. Loura, A. Fedorov, and M. Prieto. 2005. Lipid rafts have different sizes depending on membrane composition: a time-resolved fluorescence resonance energy transfer study. *J. Mol. Biol.* 346:1109–1120. doi:10.1016/j.jmb.2004.12.026

Edidin, M. 2003. The state of lipid rafts: from model membranes to cells. *Annu. Rev. Biophys. Biomol. Struct.* 32:257–283. doi:10.1146/annurev.biophys.32.110601.142439

Engisch, K.L., and M.C. Nowycky. 1998. Compensatory and excess retrieval: two types of endocytosis following single step depolarizations in bovine adrenal chromaffin cells. *J. Physiol.* 506:591–608. doi:10.1111/j.1469-7793.1998.591bv.x

Fine, M., M.C. Llaguno, V. Lariccia, M.-J. Lin, A. Yaradanakul, and D.W. Hilgemann. 2011. Massive endocytosis driven by lipidic forces originating in the outer plasmalemmal monolayer: a new

approach to membrane recycling and lipid domains. *J. Gen. Physiol.* 137:137–154.

Flewelling, R.F., and W.L. Hubbell. 1986. The membrane dipole potential in a total membrane potential model. Applications to hydrophobic ion interactions with membranes. *Biophys. J.* 49:541–552. doi:10.1016/S0006-3495(86)83664-5

Geumann, U., C. Schafer, D. Riedel, R. Jahn, and S.O. Rizzoli. 2009. Synaptic membrane proteins form stable microdomains in early endosomes. *Microsc. Res. Tech.* 73:606–616.

Gidwani, A., D. Holowka, and B. Baird. 2001. Fluorescence anisotropy measurements of lipid order in plasma membranes and lipid rafts from RBL-2H3 mast cells. *Biochemistry.* 40:12422–12429. doi:10.1021/bi010496c

Hilgemann, D.W., and A. Collins. 1992. Mechanism of cardiac Na(+)-Ca2+ exchange current stimulation by MgATP: possible involvement of aminophospholipid translocase. *J. Physiol.* 454:59–82.

Hogg, R.C., Q. Wang, and W.A. Large. 1994. Action of niflumic acid on evoked and spontaneous calcium-activated chloride and potassium currents in smooth muscle cells from rabbit portal vein. *Br. J. Pharmacol.* 112:977–984.

Jin, L., A.C. Millard, J.P. Wuskell, X. Dong, D. Wu, H.A. Clark, and L.M. Loew. 2006. Characterization and application of a new optical probe for membrane lipid domains. *Biophys. J.* 90:2563–2575. doi:10.1529/biophysj.105.072884

Kaiser, H.J., D. Linwood, I. Levental, J.L. Sampaio, L. Kalvodova, L. Rajendran, and K. Simons. 2009. Order of lipid phases in model and plasma membranes. *Proc. Natl. Acad. Sci. USA.* 106: 16645–16650.

Kenworthy, A.K. 2005. Fleeting glimpses of lipid rafts: how biophysics is being used to track them. *J. Investig. Med.* 53:312–317. doi:10.2310/6650.2005.53608

Lange, Y., J. Ye, M.E. Duban, and T.L. Steck. 2009. Activation of membrane cholesterol by 63 amphipaths. *Biochemistry.* 48:8505–8515. doi:10.1021/bi900951r

Lariccia, V., M. Fine, S. Magi, M.-J. Lin, A. Yaradanakul, M.C. Llaguno, and D.W. Hilgemann. 2011. Massive calcium–activated endocytosis without involvement of classical endocytic proteins. *J. Gen. Physiol.* 137:111–132. doi:10.1085/jgp.201010468

Levental, I., D.A. Christian, Y.H. Wang, J.J. Madara, D.E. Discher, and P.A. Janmey. 2009. Calcium-dependent lateral organization in phosphatidylinositol 4,5-bisphosphate (PIP2)- and cholesterol-containing monolayers. *Biochemistry.* 48:8241–8248. doi:10.1021/bi9007879

Lingwood, D., and K. Simons. 2007. Detergent resistance as a tool in membrane research. *Nat. Protoc.* 2:2159–2165. doi:10.1038/nprot.2007.294

Lingwood, D., and K. Simons. 2010. Lipid rafts as a membrane-organizing principle. *Science.* 327:46–50. doi:10.1126/science.1174621

Lu, C.C., A. Kabakov, V.S. Markin, S. Mager, G.A. Frazier, and D.W. Hilgemann. 1995. Membrane transport mechanisms probed by capacitance measurements with megahertz voltage clamp. *Proc. Natl. Acad. Sci. USA.* 92:11220–11224. doi:10.1073/pnas.92.24.11220

Marks, B., and H.T. McMahon. 1998. Calcium triggers calcineurin-dependent synaptic vesicle recycling in mammalian nerve terminals. *Curr. Biol.* 8:740–749. doi:10.1016/S0960-9822(98)70297-0

Mesquita, R.M., E. Melo, T.E. Thompson, and W.L. Vaz. 2000. Partitioning of amphiphiles between coexisting ordered and disordered phases in two-phase lipid bilayer membranes. *Biophys. J.* 78:3019–3025. doi:10.1016/S0006-3495(00)76840-8

Navarro, J., J. Chabot, K. Sherrill, R. Aneja, S.A. Zahler, and E. Racker. 1985. Interaction of duramycin with artificial and natural membranes. *Biochemistry.* 24:4645–4650. doi:10.1021/bi00338a025

Oberhauser, A.F., and J.M. Fernandez. 1995. Hydrophobic ions amplify the capacitive currents used to measure exocytotic fusion. *Biophys. J.* 69:451–459. doi:10.1016/S0006-3495(95)79918-0

Pickar, A.D., and W.C. Brown. 1983. Capacitance of bilayers in the presence of lipophilic ions. *Biochim. Biophys. Acta.* 733:181–185. doi:10.1016/0005-2736(83)90104-9

Plásek, J., and K. Sigler. 1996. Slow fluorescent indicators of membrane potential: a survey of different approaches to probe response analysis. *J. Photochem. Photobiol. B.* 33:101–124. doi:10.1016/1011-1344(96)07283-1

Sharma, D.K., J.C. Brown, Z. Cheng, E.L. Holicky, D.L. Marks, and R.E. Pagano. 2005. The glycosphingolipid, lactosylceramide, regulates beta1-integrin clustering and endocytosis. *Cancer Res.* 65:8233–8241. doi:10.1158/0008-5472.CAN-05-0803

Shigeno, T., M. Katakuse, T. Fujita, Y. Mukoyama, and H. Watanabe. 2009. Phthalate ester-induced thymic stromal lymphopoietin mediates allergic dermatitis in mice. *Immunology.* 128:e849–e857. doi:10.1111/j.1365-2567.2009.03094.x

Smejtek, P., and S.R. Wang. 1990. Adsorption to dipalmitoylphosphatidylcholine membranes in gel and fluid state: pentachlorophenolate, dipicrylamine, and tetraphenylborate. *Biophys. J.* 58:1285–1294. doi:10.1016/S0006-3495(90)82468-1

van der Luit, A.H., S.R. Vink, J.B. Klarenbeek, D. Perrissoud, E. Solary, M. Verheij, and W.J. van Blitterswijk. 2007. A new class of anticancer alkylphospholipids uses lipid rafts as membrane gateways to induce apoptosis in lymphoma cells. *Mol. Cancer Ther.* 6:2337–2345. doi:10.1158/1535-7163.MCT-07-0202

Wasser, C.R., M. Ertunc, X. Liu, and E.T. Kavalali. 2007. Cholesterol-dependent balance between evoked and spontaneous synaptic vesicle recycling. *J. Physiol.* 579:413–429. doi:10.1113/jphysiol.2006.123133

Wu, X.S., B.D. McNeil, J. Xu, J. Fan, L. Xue, E. Melicoff, R. Adachi, L. Bai, and L.G. Wu. 2009. Ca(2+) and calmodulin initiate all forms of endocytosis during depolarization at a nerve terminal. *Nat. Neurosci.* 12:1003–1010. doi:10.1038/nn.2355